



Residential burning is a potentially significant source of soluble iron to the ocean

Rui Li^{1,a,★}, Haley E. Plaas^{2,b,c,★}, Yifan Zhang^{1,3}, Yizhu Chen^{1,3}, Tianyu Zhang^{1,3}, Yi Yang⁴, Sagar Rathod⁵, Guohua Zhang¹, Xinming Wang¹, Douglas S. Hamilton², and Mingjin Tang^{1,6}

¹State Key Laboratory of Advanced Environmental Technology and Guangdong Key Laboratory of Environmental Protection and Resources Utilization, Guangzhou Institute of Geochemistry, Chinese Academy of Sciences, Guangzhou, China

²Marine, Earth, and Atmospheric Sciences, North Carolina State University, Raleigh, NC, USA

³College of Earth and Planetary Sciences, University of Chinese Academy of Sciences, Beijing, China

⁴Key Laboratory of Geographic Information Science of the Ministry of Education, School of Geographic Sciences, East China Normal University, Shanghai, China

⁵Department of Atmospheric, Oceanic, and Space Sciences, University of Wisconsin-Madison, Madison, WI, USA

⁶Institute of Surface-Earth System Science, School of Earth System Science, Tianjin University, Tianjin, China

^acurrent address: School of Public Health, MOE Key Laboratory of Coal Environmental Pathogenicity and Prevention, Shanxi Medical University, Taiyuan, China

^bcurrent address: Columbia University, Center for Climate Systems Research, New York, NY 10025, USA

^ccurrent address: NASA Goddard Institute for Space Studies, New York, NY, USA

★These authors contributed equally to this work.

Correspondence: Douglas S. Hamilton (dshamil3@ncsu.edu) and Mingjin Tang (mingjintang@126.com)

Received: 20 August 2025 – Discussion started: 28 August 2025

Revised: 19 May 2026 – Accepted: 28 May 2026 – Published: 26 June 2026

Abstract. Understanding the physicochemical processes that supply atmospheric aerosol iron (Fe) to the ocean is crucial for understanding of global biogeochemical cycles. Anthropogenic activity contributes significant fluxes of aerosol Fe to the atmosphere, the soluble fraction of which can modulate marine primary productivity upon its deposition to the ocean surface. However, anthropogenic aerosol Fe solubility remains poorly constrained, due in part to a lack of direct measurements spanning a multitude of anthropogenic sources. We measured solubility of aerosol Fe from several distinct anthropogenic combustion processes and fuel types. The median Fe solubility varied widely by source, ranging from 0.03 % for power plant coal fly ash to 55.87 % for biofuel burning; furthermore, residential coal burning aerosol possessed much higher Fe solubility than power plant coal fly ash. Using the new Fe solubilities reported herein, we updated parameters for anthropogenic aerosol Fe within the Community Earth System Model. Anthropogenic combustion is estimated to contribute up to 20 % of the global soluble Fe flux to the ocean in the present day. Furthermore, we identified residential coal burning as a previously neglected but potentially important source with regional flux contributions ranging from < 1 % to 21 %. Our work underscores the need to further refine understanding of aerosol Fe properties from a wide variety of anthropogenic sources by increasing observations in more novel aerosol regimes, with a focus on residential coal burning. This understanding will in turn aid in characterizing the influences of anthropogenic activity on past, present, and future atmospheric nutrient inputs to marine ecosystems.

1 Introduction

Anthropogenic activities have altered the atmospheric burden and deposition fluxes of biogeochemically relevant trace metals, including iron (Fe) (Bergas-Massó et al., 2023; Hamilton et al., 2020b). The quantity of Fe in ocean waters plays a particularly important role in modulating the spatiotemporal distribution of primary productivity in ocean ecosystems, which has downstream impacts on marine fisheries and carbon sequestration (Ito et al., 2021; Tagliabue et al., 2014, 2017). Energy-production, transportation, shipping, and manufacturing (e.g., steel production) are all characterized sources of anthropogenic aerosol Fe (Ito and Miyakawa, 2023; Ito and Shi, 2016; Rathod et al., 2024). These differing combustion fuel types possess distinct physicochemical properties that influence their impact on radiative forcing and nutrient supply (Al-Abadleh et al., 2023; Ito et al., 2018; Matsui et al., 2018; Rathod et al., 2020).

To assess the potential nutritional impact of atmospheric Fe deposition on ocean ecosystems, atmospheric aerosol research primarily focuses on tracing the soluble Fe content in aerosol (Baker et al., 2020; Ito et al., 2019; Mahowald et al., 2018). Soluble Fe content is often expressed as the fraction of soluble to total Fe in aerosol and then reported as a percentage solubility (Baldo et al., 2022; Liu et al., 2022; Mahowald et al., 2009). Several key processes control solubility of aerosol Fe over the course of its lifetime: (1) Fe mineralogy, (2) interactions with acidic and organic species in aerosol and cloud water, and (3) particle size and surface area to volume ratios (Bergas-Massó et al., 2023; Journet et al., 2008; McDaniel et al., 2019). Anthropogenic combustion not only alters the magnitude and spatial distribution of Fe fluxes from the atmosphere and to the surface ocean, but also influences the composition of the atmosphere, that in turn, influences dissolution chemistry of aerosol Fe both directly and indirectly. Mixing of aerosol Fe with acidic (e.g., sulfates or nitrates) and organic species (e.g., oxalate) co-emitted during anthropogenic combustion increases its solubility during transport (Bergas-Massó et al., 2023; Chen et al., 2024; Itahashi et al., 2022; Li et al., 2017; Longo et al., 2016). Furthermore, diverse technologies utilized during combustion processes (i.e., variable combustion temperatures, boilers vs. furnaces, degree of emission control, and the fuel quality) also influence the physicochemical properties of aerosol Fe beyond the composition of fuel alone. As a result, studies examining socioeconomic, technology, and policy driven changes to anthropogenic fuel-burning are needed to anticipate impacts on the global Fe cycle (Hamilton et al., 2020b).

When compared to mineral dust, anthropogenic emissions of aerosol Fe are several orders of magnitude lower at the global scale; however, anthropogenic Fe has a higher fractional solubility (Ito et al., 2021), and the relative contribution of soluble Fe from anthropogenic combustion is spatially distinct from dust (Hamilton et al., 2020b, 2019). Therefore,

anthropogenic activity can be a major contributor to Fe fluxes in many high nutrient low chlorophyll (HNLC) ocean regions (Hawco et al., 2025; Liu et al., 2022).

Despite the importance of understanding anthropogenic Fe fluxes, the fractional solubility of aerosol Fe emitted from various anthropogenic sources remains poorly understood (Desboeufs et al., 2005; Li et al., 2022b; Oakes et al., 2012); consequently, Fe solubility parameterizations in modeling studies for anthropogenic Fe vary widely (Ito et al., 2019; Myriokefalitakis et al., 2018). In this work, we measured the Fe content and solubility for aerosol emitted by several important anthropogenic sources (i.e., coal power plants, steelwork industry, municipal waste combustion, oil combustion, residential coal, and biofuel burning). Then, using an Earth System Model, we applied the experimental results by updating Fe solubility parameters for distinct anthropogenic combustion fuel-sources. Simulated Fe concentrations and solubilities were validated against a global observational Fe aerosol dataset at the regional scale. Then, the model was used to quantify and bound uncertainties in emission and deposition fluxes of soluble Fe under three anthropogenic combustion emission scenarios spanning past (pre-industrial) to future (Shared Socioeconomic Pathway 3-7.0, SSP370) conditions.

2 Methodology

The experimental and modelling methods employed in this work are described in Sect. 2.1 and 2.2, respectively.

2.1 Experimental methods

This work examined six types of anthropogenic combustion aerosol, which were classified into two broad categories. The first category, fly ash, included power plant coal fly ash, steelwork fly ash, municipal waste fly ash, and oil fly ash. The second category, residential fuel sources, included residential coal and biofuel combustion. Biofuels examined in this work were limited to straw, wood, grasses and leaves, and we did not examine other biofuels such as dung.

2.1.1 Fly ash and bottom ash samples

The volume-mean diameters, determined using diameter light scattering, were found to be 16.9–67.6, 4.7–176.4, 21.2–115.9 and 15.4 μm for power plant coal fly ash ($n = 31$), steelwork fly ash ($n = 29$), municipal waste fly ash ($n = 3$), and oil fly ash ($n = 1$) samples, respectively (Li, 2025).

Power plant coal fly ash samples were obtained from electrostatic precipitators or baghouse rows in coal power plants in 29 provinces in China (Li et al., 2021; Liu et al., 2021); one coal power plant was selected in each province except for Guangdong and Shandong where two coal power plants were selected for each province. As a result, 31 power plant coal fly ash samples were examined in total. In addition, we

examined 29 steelwork fly ash samples collected from different iron and steel plants, three municipal waste fly ash samples (Li et al., 2022b, 2021), and two oil fly ash samples which were PM_{2.5} samples emitted by heavy oil and diesel fuel combustion in the engine of a cargo ship (Wu et al., 2018), and one oil bottom ash sample (Fu et al., 2012). As the numbers of municipal waste and oil ash samples were limited, we include their results data in the Supplement, but do not discuss them further in the main paper due to a lack of statistical significance.

Fly ash and bottom ash samples (~ 10 mg for each sample) were digested and then analyzed using inductively coupled plasma mass spectrometry (ICP-MS) to determine their Fe content. Experimental procedures for sample digestion and total Fe measurement can be found elsewhere (Li et al., 2022c). Soluble Fe was leached and determined using the procedure described in our previous work (Li et al., 2022b). In brief, fly ash and bottom ash samples (~ 20 mg for each sample) were individually leached in 20 mL sodium acetate buffer (5 mmol L⁻¹, pH = 4.3) for 2 h, during which an orbital shaker (300 rpm) was used to stir the solution. The aqueous mixture was centrifuged (3000 rpm) for 15 min, and a pH paper (range: 3.5–6.8; precision: 0.3; Macherey-Nagel, Germany) was used to measure the pH of the solution and no measurable pH change occurred after leaching. The aqueous solution was filtered through a polyethersulfone filter (pore size: 0.22 µm), acidified to contain 1 % (v/v) nitric acid and then analyzed by ICP-MS to measure soluble Fe. In this work, fractional solubility of Fe was reported as the ratio (in %) of soluble Fe to total Fe.

A wide range of protocols, differing in leaching solution, filter pore size, and so on, were used to extract soluble Fe, and the results obtained using different leaching protocols could be substantial (Tang et al., 2025). Sodium acetate buffer, instead of ultrapure water, was used in the present work as the leaching solution, because its pH did not change during leaching due to its larger buffering capacity compared to ultrapure water.

2.1.2 Residential coal and biofuel combustion aerosols

Generation and collection of residential coal and biofuel combustion aerosols are detailed in the Supplement (Sect. S1 in the Supplement). In brief, we burned coal and biofuel in a commercial cook stove widely used in rural areas in China and collected PM_{2.5} samples (aerosol particles with aerodynamic particle diameters below 2.5 µm) onto pre-cleaned Whatman 41 (W41) cellulose filters using a medium volume aerosol sampler (TH-150C, Tianhong Co.).

Our work examined three types of coal (anthracite, semibituminous coal, and bituminous coal) and nine types of biofuel (wheat straw, rice straw, corn straw, rape straw, cogongrass, China fir trunk, pine trunk, poplar trunk, and pine needle) commonly found in China. We collected eight filter samples for each fuel type, except anthracite for which we

only collected two filter samples. We had to combine some filter samples in our experimental analysis to meet the detection limit for soluble Fe; as a result, the number of effective filter samples (for which Fe content and solubility were reported) were usually < 8 for each fuel type (see Tables S2 and S4 for further information).

After aerosol collection, the filters were individually placed in a pre-cleaned Petri dish and then stored in a desiccator for 60 h to remove particle-associated water. The mass of filters before and after aerosol collection were measured (accuracy of 0.1 mg), and the mass of particles collected ranged from 2.5 to 432.7 mg. Each filter was then divided into two equal parts. To determine the soluble Fe content, the first half of a filter was leached in 20 mL sodium acetate buffer (5 mmol L⁻¹, pH = 4.3) for 2 h (Sect. 2.1.1) and analyzed using ICP-MS. Fe concentrations in some leaching solutions were low; as a result, these leaching solutions (~ 15 mL for each solution) were combined for the same fuel type and then pre-concentrated to a volume of 6 mL, in order to increase Fe concentration in the solution used for ICP-MS analysis. The second half of a filter was digested and analyzed by ICP-MS to determine total Fe, and the experimental procedure used can be found in our previous work (Zhang et al., 2022). If leaching solutions were combined for the first parts of these filters, their second parts were also combined and digested together to allow direct comparison.

2.1.3 Quality assurance and quality control

The detection limit of Fe in solution was determined to be 0.5 µg L⁻¹ in this work. A reference solution (NIST 1643f) was used to check the accuracy of ICP-MS analysis, and the difference between actual and measured concentrations was found to be < 1 %. Furthermore, three blanks (with no fly ash or filters not loaded with any particles) were used in each batch when we measured total or soluble Fe. The background levels of soluble Fe were always below the detection limit; the background levels of total Fe, ranging from 4.3–5.7 µg L⁻¹, were much lower than total Fe concentrations for most of our samples and subtracted when we reported our results.

2.2 Model simulations

2.2.1 Atmospheric Fe model description

Earth System Models can investigate the spatiotemporal distribution and fluxes of key atmospheric nutrients under various climatological regimes (Hamilton et al., 2020b, 2022; Wu et al., 2020). To test the impact of new soluble Fe parameters (Sect. 2.1) on modeled fluxes of soluble aerosol Fe to the atmosphere and marine ecosystems, we used the Mechanism of Intermediate complexity for Modeling Iron (MIMI). MIMI is an Fe aerosol-chemistry module embedded within the atmospheric component (Community Atmosphere Model version 6, CAM6) of the Community Earth System

Model version 2 (CESM2) (Danabasoglu et al., 2020; Hamilton et al., 2019). Mineral dust, anthropogenic combustion, and wildfire emissions are currently represented as distinct sources of aerosol Fe in MIMI. The current dust emission scheme within MIMI includes an updated soil moisture submodule within the land component of the model that prognostically calculates dust aerosolization as a function of soil moisture (Li et al., 2022a). Following the implementation of a new soil-moisture scheme, dust was rescaled to attain a global climatological mean dust aerosol optical depth of ~ 0.03 (Ridley et al., 2016), consistent with all previous versions of the MIMI model. The inclusion of these improvements to dust and updated anthropogenic Fe sources represents a new working version of MIMI v1.1, as described herein, and detailed validation efforts are reported in the Supplement (Fig. S3 and Table S13).

A comprehensive overview of model details and parameters is provided in Hamilton et al. (2019); in brief, MIMI simulates the emission, atmospheric transport, and deposition of Fe-containing aerosol within three distinct particle size modes (Aitken, accumulation, and coarse modes). Within each source of aerosol Fe (dust, wildfire, and anthropogenic combustion), both the insoluble and soluble fractions are carried as separate tracers, and the soluble fraction of Fe for each aerosol source is assigned at the point of emission. Prior to deposition and during atmospheric transport, Fe solubility is further modified via non-reversible multiphase reactions with acidic and organic species. Acidic processing is a function of aerosol pH and temperature (Meskhidze et al., 2005), while organic processing is an aqueous phase chemistry reaction that depends on oxalate concentrations which are calculated based on the concentrations of secondary organic aerosol present (Johnson and Meskhidze, 2013; Scanza et al., 2018).

The model is gridded in a 3-dimensional space at a resolution of $0.96 \times 1.25^\circ$ (latitude \times longitude) and includes 56 vertical pressure levels from the surface to 2 hPa at the highest altitude. Meteorology is forced in all the simulations using Modern-Era Retrospective analysis for Research and Applications Version 2 (MERRA-2), and a 1-year model spin up was undertaken for all simulations.

2.2.2 Global pyrogenic Fe emission inventories and input dataset development

While dust Fe emissions are calculated prognostically within MIMI, anthropogenic and wildfire (sum of these being pyrogenic) emissions are prescribed using emissions inventories. Annual mean anthropogenic Fe emission fluxes were inputted to the model using a modified version of an inventory first developed in Rathod et al. (2020) and further detailed in Rathod et al. (2024). In this inventory, Fe content in combustion aerosol was empirically derived for the present day (PD; climatological year 2010) using the Speciated Pollution Emissions Wizard (SPEW) (Bond et al., 2007, 2004),

which characterizes anthropogenic emissions of particulate matter by fuel-source and combustion technology. Soluble and insoluble Fe content are dependent on fuel-type and also segregated by key sectors: (1) industrial fossil fuel (coal), (2) industrial and vehicular fossil fuels (oil), (3) smelting operations (steel/iron), (4) cooking/heating using biomass (bio-fuel/wood), and (5) waste burning (Rathod et al., 2020). Industrial oil emissions were separated by land- and sea-based emissions to distinguish terrestrial transportation from shipping. Wildfire-Fe emission parameters are detailed in Hamilton et al. (2019), and in this work we used the CMIP6 (Coupled Model Intercomparison Project phase six) fire emission inventory for PD simulations (van Marle et al., 2017).

Here, for the first time, we separated anthropogenic coal Fe into distinct industrial and residential sources and tested three approaches to constrain the magnitude of the residential Fe signal, i.e. a high, central-high, and central-residential emission scenario, with the naming conventions relative to the residential Fe emissions reported by Rathod et al. (2020, 2024). Each inventory increases in its respective source grouping complexity to evaluate key uncertainties in the representation of Fe emissions from residential combustion in global inventories (Figs. 1, S4 and S5; Table S8). Key to this process is the mapping fuel-specific Fe emissions to CMIP6 anthropogenic sectors, enabling future projections of sector-specific emission changes under the SSP scenarios. The CMIP6 anthropogenic emission dataset as detailed in Hoesly et al. (2018) classifies anthropogenic emission sectors as: (0) agriculture, (1) energy, (2) industrial, (3) terrestrial transportation, (4) residential/commercial/other, (5) solvents production/application, (6) waste, and (7) international shipping.

To create the first emission inventory (“high-residential”), we multiplied a series of spatially-resolved ($1^\circ \times 1^\circ$ grid box) ratios of residential-to-industrial black carbon (BC) emissions to the Rathod et al. (2024) Fe inventory emissions for coal. Hoesly et al. (2018) do not separate biofuel (wood) from residential coal (Table S8); in order to reflect an upper limit for residential coal burning, we treated all of CMIP6 Sector #4 (residential, commercial, and other) BC as the residential coal fraction and CMIP6 Sectors #1 + 2 (energy + industrial) BC as the industrial coal fraction (Fig. S4; Eqs. 1a and 1b) (Hoesly et al., 2018):

$$[\text{Fe}_{\text{RESI}}]_{i,j,\text{HIGH}} = \frac{[\text{BC}_{\text{RESI}}]_{i,j,\text{H}}}{[\text{BC}_{\text{RESI}+\text{IND}}]_{i,j,\text{H}}} \times [\text{Fe}_{\text{IND}+\text{RESI}}]_{i,j,\text{R}} \quad (1a)$$

$$[\text{Fe}_{\text{IND}}]_{i,j,\text{HIGH}} = \frac{[\text{BC}_{\text{IND}}]_{i,j,\text{H}}}{[\text{BC}_{\text{RESI}+\text{IND}}]_{i,j,\text{H}}} \times [\text{Fe}_{\text{IND}+\text{RESI}}]_{i,j,\text{R}} \quad (1b)$$

Where i and j represent the longitudinal and latitudinal coordinates, RESI and IND represent residential and industrial sources, HIGH represents the high-residential inventory being constructed, H represents the Hoesly et al. (2018) dataset, R represents the Rathod et al. (2024) dataset, and [Fe] and [BC] represent their respective speciated fluxes in units of

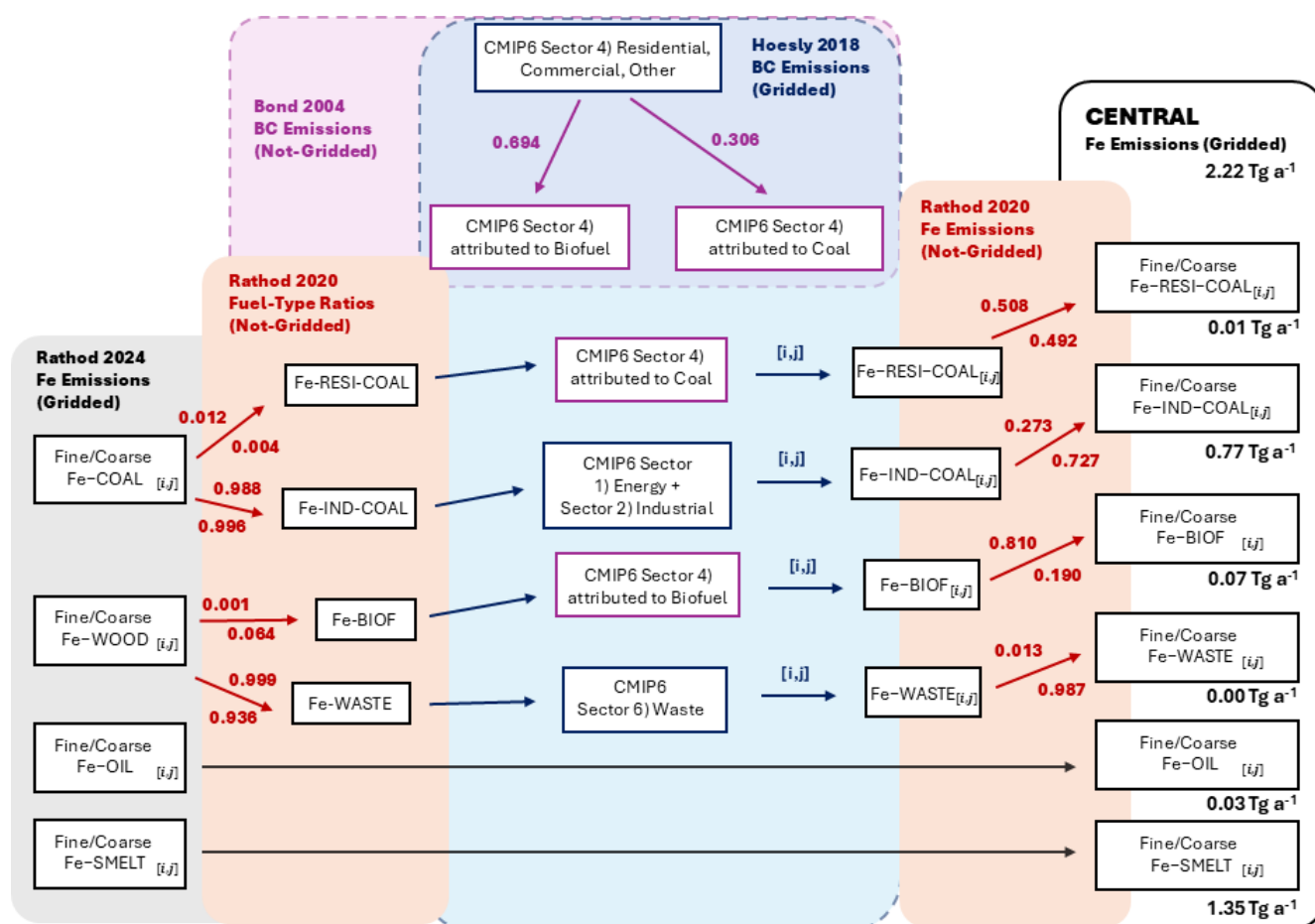


Figure 1. A flowchart representing the steps followed and datasets leveraged to create the central-anthropogenic Fe emissions inventory. Dashed lines indicate a BC dataset, and solid/no outlines indicate an Fe dataset. Two values are provided with each red line to show the fractional split between fine and coarse fractions; the above arrow indicates the fine fraction, while the below values indicates the coarse fraction. Similar flowcharts for the central-high and high- inventories are provided in Figs. S4 and S5.

$\text{kg m}^{-2} \text{s}^{-1}$. This approach was chosen to capture spatial variations in coal burning technologies within the inventory but assumed that residential Fe-to-industrial Fe emissions track residential BC-to-industrial BC by grid cell.

To create the second emission inventory (“central-high-residential”) we globally scaled the high-residential inventory to reflect global Fe emission budgets from residential coal burning sources previously reported in Rathod et al. (2020). Using the ratio of residential coal to all residential sources reported in Bond et al. (2004) and assuming parity between BC datasets, we estimated the portion of CMIP6 Sector #4 BC that could be attributed to residential coal burning (Table S8). Then, we redistributed the Fe emissions in the high inventory between residential and industrial coal to reflect this using a global scaling factor of 0.035 (residential:industrial), constituting the central-high inventory (Fig. S5).

To create the third emission inventory (“central-”), rather than using the Hoesly et al. (2018) BC data to separate

residential from industrial coal emissions, we determined the fractional contribution of residential + commercial Fe to total coal-Fe emissions reported in Rathod et al. (2020) (commercial and residential sources were specifically grouped to track CMIP6 Sector #4; Fig. 1). This separation was applied uniformly at the global scale for each of the fine and coarse aerosol modes individually. The sector-specific ratio of Fe : BC was then applied to map spatial heterogeneity in emissions following the CMIP6 emissions data (Fig. 1), where sector-specific BC was taken from Hoesly et al. (2018). Sector #4 (Residential, Commercial, Other) BC emissions were again split into residential coal vs. biofuel sources using Bond et al. (2004) (Fig. 1; Table S8). To best track CMIP6 groupings, we treated “energy” and “industrial” sources together as industrial coal, “waste” sources as waste, and ocean-masked “international shipping” with land-masked “terrestrial transportation” together as oil BC sources. Finally, fine and coarse mode Fe emissions were re-

distinguished following the fuel-specific global averages reported in Rathod et al. (2020) (Fig. 1).

The central-, central-high, and high-residential coal emissions span three orders of magnitude at the global scale (4.9, 16, and 460 Gg a⁻¹, respectively; Table S9). Each inventory was applied and tested with each PD model simulation to perform a sensitivity analysis that quantified the uncertainty in residential coal Fe emissions introduced by each new inventory. To capture the lower and upper bounds of uncertainty associated with residential-Fe emissions, herein we present results from the high and central- inventories only; results from the central-high inventory are provided in the Supplement.

Once sector-specific emissions inventories were read into the model, fuel-sources were summed to total one anthropogenic tracer. This tracer is then separated into soluble and insoluble fractions with three modes within the model code (Eqs. 2a and 2b). This results in six anthropogenic combustion-Fe tracers in total to be transported within the model, as follows:

$$[\text{Fe}_{\text{insol}}]_a = \Sigma \{ [\text{Fe}_X]_{i,j,a,b} \times (1 - \text{sol}_b) \} \quad (2a)$$

$$[\text{Fe}_{\text{sol}}]_a = \Sigma ([\text{Fe}_X]_{i,j,a,b} \times \text{sol}_b) \quad (2b)$$

where X denotes the emissions scenario, a represents the aerosol mode (fine or coarse), b represents the fuel-source (industrial oil, industrial coal, residential coal, biofuel, or smelting), insol represents the insoluble fraction, sol represents the soluble fraction, and sol_b represents the fractional solubility for each fuel-source (b). As a final step, the fine mode was split into accumulation and Aitken modes by applying a ratio of 9 : 1.

2.2.3 Model simulations performed

Sixteen model simulations were performed to evaluate the impact of anthropogenic combustion aerosol solubility updates (Sect. 2.1) on atmospheric soluble Fe fluxes to key marine ecosystems (Table 1). For all simulations, we set the model climatology to present-day (PD) conditions, spanning 2009–2011 inclusive. Simulations were distinguished as cases (variable Fe solubility parameterizations) within different emission scenarios (variable anthropogenic combustion emission fluxes).

The first ten simulations (i.e., PD simulations) aimed to assess the impact of each new solubility parameter on the ability of the model to capture ship-based observations of total Fe, soluble Fe, and Fe solubility. These simulations applied the high-residential emissions inventory (Sect. 2.2.2) and were repeated using the central-residential Fe inventory with the exception of PD-IND (Table 1). The first PD case in each set (i.e., PD-BASE) served as a baseline, i.e., no changes were made to solubility when compared to previous studies using MIMI. Residential coal was distinguished from industrial coal emissions, but this had no impact on soluble

Fe fluxes since the same fractional solubility (0.2 %) was applied to both sources (Rathod et al., 2020, 2024). In the next three PD cases (PD-RESI, PD-BIOF, PD-IND), fractional solubility was updated incrementally for individual sectors to assess fuel-type specific impacts to soluble Fe fluxes, which are later detailed in Sect. 3.3; results from PD-IND are reported in the Supplement. Information on model validation and constraint to ship-based observations of aerosol Fe is provided in Sect. 2.2.5.

Using both pre-industrial (PI; 1750 CE) and future (FU; 2050 and 2100 CE) anthropogenic emissions scenarios, we performed six model simulations to examine the impacts of changes in anthropogenic activity on Fe fluxes over time. In each pair of simulations, we applied the -BASE solubility parameters to establish a baseline and the -BIOF solubility parameters to examine an upper bound for residential soluble Fe fluxes. Accordingly, we also used the high-residential Fe emissions inventory framework in development of the FU emissions inventory to further establish a maximum estimate for anthropogenic soluble Fe through the end of the 21st century. To isolate how changes in soluble aerosol Fe fluxes responded to changes in emission parameterizations and subsequent dissolution chemistry in the model, PI and FU simulations were conducted with meteorological and climatological conditions identical to the PD (2009–2011).

The PI simulations (PI-BASE and PI-BIOF) served as a reference point for comparison to PD and FU simulations, per minimal influence on the Fe cycle by anthropogenic emissions (Table 1). MID-SSP370-BASE, MID-SSP370-BIOF, END-SSP370-BASE, and END-SSP370-BIOF were conducted to evaluate the projected impact of population increases and socioeconomic changes to energy production and fuel-usage over the course of the century. We selected the highest air pollution emissions scenario of the Shared Socio-economic Pathways (SSPs) as detailed in SSP 3-7.0 (SSP370), the “regional rivalry” scenario, which represents anticipated sociopolitical and environmental changes resulting in an increase to radiative forcing by 3–7.0 W m⁻² by the year of 2100 (Riahi et al., 2017). Given that BC emissions are anticipated to peak in the midcentury (2040–2050) but return to PD-comparable emissions by 2100 (Turnock et al., 2020), we assessed projected changes to Fe emissions at both the mid-point (2050) and endpoint of the 21st century (2100). Dust fluxes in future Fe emission scenarios were adjusted to account for dust-climate feedback using a scaling factor ranging between 1.0–1.1, as described in Hamilton et al. (2020a).

2.2.4 Preindustrial (PI) and future (FU) Fe emission estimates

For PI simulations, we used a pre-developed Fe combustion emission inventory (Hamilton et al., 2020b). Only residential (wood) biofuel burning served as an anthropogenic source of Fe due to a presumable lack of industrialized an-

Table 1. Description of model simulations performed using MIMI with emission scenarios and emission inventories either directly input (Fe) to the model or utilized to generate the Fe inventory (BC). PD = present day (2010 CE), PI = pre-industrial (1750 CE), SSP370 = Shared Socioeconomic Pathway scenario 3-7.0, MID = midcentury (2040–2050 CE) and END = end century (2090–2100 CE). NA = assumed industrial activity is zero at 1750 CE. Note the BC budget varies for the central- inventory per the inclusion of waste sources.

Emissions Scenario	Simulation	Fe Emissions Inventory	BC Emissions database	BC Emission (Tg a^{-1})
PD	PD-BASE	Rathod et al. (2024)	Hoesly et al. (2018)	6.46
PD	PD-RESI	High-Residential	Hoesly et al. (2018)	6.46
PD	PD-BIOF	High-Residential	Hoesly et al. (2018)	6.46
PD	PD-IND	High-Residential	Hoesly et al. (2018)	6.46
PD	PD-BASE	Central-High-Residential	Bond et al. (2004) & Hoesly et al. (2018)	6.46
PD	PD-RESI	Central-High-Residential	Bond et al. (2004) & Hoesly et al. (2018)	6.46
PD	PD-BIOF	Central-High-Residential	Bond et al. (2004) & Hoesly et al. (2018)	6.46
PD	PD-BASE	Central-Residential	Bond et al. (2004) & Hoesly et al. (2018)	6.97
PD	PD-RESI	Central-Residential	Bond et al. (2004) & Hoesly et al. (2018)	6.97
PD	PD-BIOF	Central-Residential	Bond et al. (2004) & Hoesly et al. (2018)	6.97
PI	PI-BASE	Hamilton et al. (2020a)	NA	NA
PI	PI-BIOF	Hamilton et al. (2020a)	NA	NA
FU (2050)	MID-SSP370-BASE	High-Residential	SSP3.70	8.30
FU (2050)	MID-SSP370-BIOF	High-Residential	SSP3.70	8.30
FU (2100)	END-SSP370-BASE	High-Residential	SSP3.70	6.33
FU (2100)	END-SSP370-BIOF	High-Residential	SSP3.70	6.33

thropogenic emissions (i.e., fossil fuels and smelting; Hamilton et al., 2020a); global emission for anthropogenic combustion was $0.7 \times 10^{-3} \text{ Gg Fe a}^{-1}$ and only occupied the fine aerosol mode (i.e., sum of Aitken and accumulation modes). Details on the development of the PI Fe combustion emission inventory are provided in Hamilton et al. (2020b).

For FU simulations, we developed two new Fe emissions datasets (for 2050 and 2100) which were both derived from our high-residential emissions inventory developed for the PD simulations. Fe emissions were linearly scaled for all combustion sources according to projected changes in anthropogenic BC emissions via the decadal CMIP6 anthropogenic BC emission dataset for 2040–2050 and 2090–2100 (Hoesly et al., 2018; Riahi et al., 2017). BC emissions labeled “residential, commercial and other” were separated into residential coal and residential biofuel sources of BC based on

the grid-cell specific ratios of residential coal Fe to residential biofuel Fe in our high-residential emissions inventory.

Following a similar approach to the PD high-residential emissions inventory, using a grid-cell resolved dynamic ratio of Fe-to-BC, that was grouped based on sector and aerosol size fraction, we calculated FU Fe emissions tracking CMIP6 projected BC emissions (Eq. 3), as follows:

$$\frac{[\text{Fe}_X]_{i,j,a,b}}{[\text{BC}_X]_{i,j,a,b}} = \frac{[\text{Fe}_{\text{PD}}]_{i,j,a,b}}{[\text{BC}_{\text{PD}}]_{i,j,a,b}} \quad (3)$$

where X denotes the emissions scenario (MID-SSP370 or END-SSP370), i and j represent the longitudinal and latitudinal coordinates, a represents the aerosol mode (fine or coarse), b represents the fuel-source (industrial oil, industrial coal, residential coal, biofuel, or smelting), and $[\text{Fe}]$ and $[\text{BC}]$ represent the speciated fluxes ($\text{kg m}^{-2} \text{ s}^{-1}$). BC emissions from smelting operations were not directly available for

PI or FU projections; therefore, they were set to 0.0 in the PI and maintained at PD levels in the FU. By using SSP370, the -BIOF case solubility parameters, and the high-residential emissions inventory, our FU simulations established an upper bound estimate for future anthropogenic soluble Fe fluxes as based on current observational uncertainties. The SimFire inventory, coupled to the LPJ-GUESS (Lund-Potsdam-Jena General Ecosystem Simulator) vegetation model, was used to prescribe wildfire-Fe emissions during the PI era (Hamilton et al., 2018, 2020a; Knorr et al., 2016). For wildfire-Fe emissions in FU scenarios, we used the CMIP6 fire emission datasets for MID-SSP370 and END-SSP370 (Bergas-Masso et al., 2025; Hamilton et al., 2024).

2.2.5 Model validation

To evaluate model performance, we compared global observations of total Fe concentration, soluble Fe concentration, and Fe solubility to modeled values for each PD simulation, grouping data by key aerosol deposition and ocean biogeochemistry regions. The observational dataset of Fe content in aerosol was reported in Hamilton et al. (2019) and updated herein to include measurements from Srinivas et al. (2012) and more recent studies published between 2021 and 2024 ($n = 1624$) (Desboeufs et al., 2024; Elliott et al., 2024; Kurisu et al., 2021; López-García et al., 2021; Marafante et al., 2024; Panda et al., 2022; Perron et al., 2022; Rodríguez et al., 2021; Sakata et al., 2022; Seo and Kim, 2023; Winton et al., 2022; Wu et al., 2023; Zhang et al., 2024).

Observed Fe solubility in aerosol spans five orders of magnitude (Perron et al., 2024), and one reason for this large range is due to differences in experimental procedures during quantification (Tang et al., 2025). To facilitate a more direct comparison between modeled and observed soluble Fe content, we removed observations from the global dataset that did not measure soluble Fe directly. When multiple observations fell within a model grid cell, values were aggregated to climatological averages, using medians to be most representative of expected variations in Fe fluxes across time and space (final $n = 990$; Fig. 2). For final evaluation of the model capability in simulating surface Fe concentrations, both model and observational data were grouped into key ocean regions (Fig. 2), based on predominant sources of atmospheric aerosol and phytoplankton nutrient limitation dynamics (i.e., HNLC regions) as revealed in Hamilton et al. (2019, 2023). To quantitatively evaluate model skill, root mean square errors (RMSE) were calculated for the high-residential inventory cases and are provided in the Supplement.

3 Results and Discussion

Section 3.1 and 3.2 present Fe content and solubility measured in our experimental work. The numbers of samples examined in our work are very small for municipal waste fly

ash and oil fly/bottom ash, and the results may not be representative; therefore, these results are mainly presented in the Supplement. Modeling results are presented in Sect. 3.3.

3.1 Fe content by fuel type

This work quantified the Fe content in particles from six different combustion and anthropogenic sources, including power plant coal fly ash, residential coal combustion aerosol, steelwork fly ash, residential biofuel burning aerosol, municipal waste fly ash, and oil fly ash (Table 2; Fe content in individual samples is provided in Tables S1–S5).

3.1.1 Power plant coal fly ash

Fe content ranged from 20.7 to 103.8 mg g⁻¹ for the 31 power plant coal fly ash samples examined in our work, with average and median values being 37.2 ± 16.8 and 35.0 mg g⁻¹, respectively. As shown in Table S6, Fe content ranged from 16.0 to 52.0 mg g⁻¹ ($n = 3$) in one study (Baldo et al., 2022), with mean and median values being 33.0 ± 18.0 and 31.0 mg g⁻¹; in another study (Goodarzi, 2006), the median value of Fe content was determined to be 34.4 mg g⁻¹ ($n = 7$). Fe content measured by these two studies (Baldo et al., 2022; Goodarzi, 2006) agreed well with our work. Some other studies (Dutta et al., 2009; Fu et al., 2012; Jankowski et al., 2006; Meij, 1994) found higher mean or median Fe content for power plant coal fly ash (Table S6), but the reported ranges overlapped with our work. For example, Fe content were found to range from 38.3 to 98.6 mg g⁻¹ ($n = 7$) in one study (Li et al., 2022b), with mean and median values being 62.1 ± 26.7 and 43.2 mg g⁻¹; in another study (Moreno et al., 2005), Fe content were found to range from 18.2 to 112.0 mg g⁻¹ ($n = 23$), with mean and median values being 57.8 ± 22.7 and 52.5 mg g⁻¹.

In summary, the mean or median Fe content reported in different studies are typically in the range of 30–70 mg g⁻¹ for power plant coal fly ash, and this variability is likely due to difference in coal (Wang et al., 2015; Ward, 2016) and combustion conditions (Blissett and Rowson, 2012; Kutchko and Kim, 2006). Fe content in power plant coal fly ash was set to ~70 mg g⁻¹ in some modeling studies (Luo et al., 2008; Rathod et al., 2020), being consistent with experimental results.

3.1.2 Residential coal combustion aerosol

For the 10 residential coal combustion aerosol samples (PM_{2.5}) we examined, Fe content ranged from 0.025 to 0.101 mg g⁻¹ (Table 2), with average and median values being 0.044 ± 0.023 and 0.038 mg g⁻¹, respectively. Only a few previous studies measured Fe content in residential coal combustion aerosols (Table S6). The average Fe content was determined by Patil et al. (2013) to be 0.048 ± 0.035 mg g⁻¹ ($n = 3$) for PM_{2.5} and 0.061 ± 0.044 mg g⁻¹ ($n = 3$) for

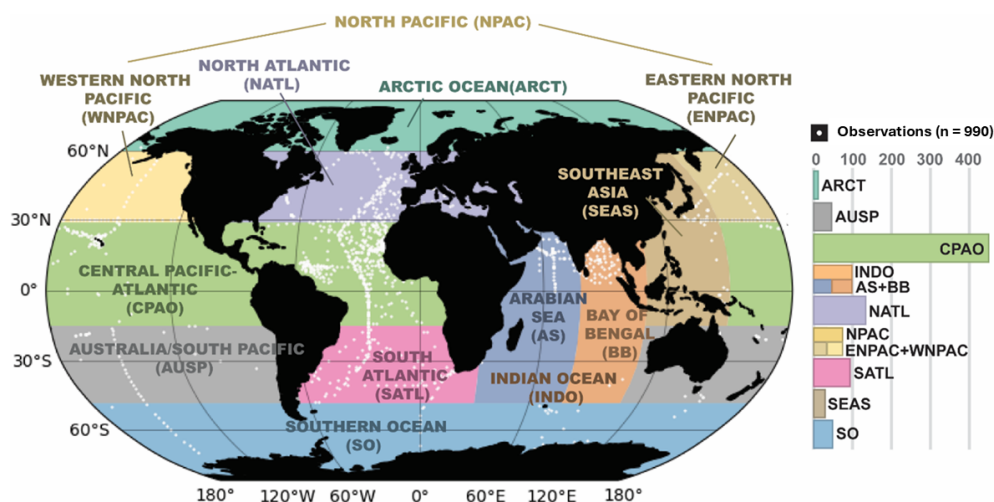


Figure 2. Regional groupings for model-observation comparisons of surface Fe concentrations (ship-based, in aerosol). The coordinates for individual Fe observations are indicated with a white circle. Number of soluble Fe observations within each region are provided by the histogram ($n = 990$).

Table 2. Summary of Fe content and solubility for power plant coal fly ash, residential coal combustion aerosol, steelwork fly ash, and biofuel burning aerosol examined in our work (n : number of samples examined in our work). Fe content and solubility for other samples examined in this work (i.e. municipal waste fly ash, oil fly ash and oil bottom ash) can be found in the Supplement.

sample type	n	range	average	median
Fe content (mg g^{-1})				
power plant coal fly ash	31	20.7–103.8	37.2 ± 16.8	35.0
residential coal combustion aerosol	10	0.025–0.101	0.044 ± 0.023	0.038
steelwork fly ash	29	5.8–918.9	312.6 ± 246.1	346.5
biofuel burning aerosol	27	0.002–0.101	0.023 ± 0.026	0.013
Fe solubility (%)				
power plant coal fly ash	31	0.002–0.17	0.05 ± 0.05	0.03
residential coal combustion aerosol	10	7.03–100	33.30 ± 27.71	28.45
steelwork fly ash	29	0.007–10.64	1.37 ± 2.77	0.07
biofuel burning aerosol	28	2.86–100	56.07 ± 30.95	55.87

PM₁₀, being similar to or slightly higher than our result. In another two studies (Watson et al., 2001; Zhang et al., 2012), the average Fe content was measured to be $0.671 \pm 0.023 \text{ mg g}^{-1}$ ($n = 4$) and $0.7 \pm 0.1 \text{ mg g}^{-1}$ ($n = 5$), significantly higher than our result, and such differences may be attributed to variations in coal types and combustion conditions. Overall, our and previous studies suggest that the Fe content in residential coal combustion aerosols is very low, typically below 1 mg g^{-1} . Fe content were set to 1 and 0.5 mg g^{-1} in previous modeling studies (Luo et al., 2008; Rathod et al., 2020), being broadly consistent with experimental results.

Fe content in power plant coal fly ash is much higher than residential coal combustion aerosols, primarily due to differences in combustion conditions (Rathod et al., 2020). Power plant coal fly ash has very low carbon content and is mainly composed of metals and minerals (Ahmaruzzaman, 2010; Li

et al., 2022c; Patil et al., 2013); in contrast, residential coal combustion aerosol particles contain a large fraction of carbonaceous materials due to incomplete combustion, and thus the content of metals, including Fe, are much lower (Patil et al., 2013; Zhang et al., 2012). Furthermore, combustion temperature typically ranges from 1200 to 1700 °C for coal-fired power plant, enabling Fe in coal to enter fly ash particles through volatilization-condensation (Blissett and Rowson, 2012); residential coal combustion occurs at much lower temperatures which are insufficient for Fe to enter aerosols through this process (Rathod et al., 2020), also leading to lower Fe content.

3.1.3 Steelwork fly ash

For the 29 steelwork fly ash samples we examined, Fe content ranged from 5.8 to 918.9 mg g⁻¹, with mean and median values measured to be 312.6 ± 246.1 and 346.5 mg g⁻¹, respectively (Table 2). As shown in Table S6, some previous studies have reported average Fe content to be 358.9 (*n* = 1), 369.3 (*n* = 1), 312.2 (*n* = 1), and 329.1 ± 22.6 mg g⁻¹ (*n* = 4) (Alizadeh and Momeni, 2016; Silva et al., 2019; Souza et al., 2010; Vieira et al., 2013), in good agreement with our results. Lower Fe content was also reported by previous work, with average values being 86.0 (*n* = 1), 128.1 (*n* = 1), 150.8 (*n* = 1), 286.5 (*n* = 1), 284.6 (*n* = 1), 238.7 (*n* = 1), and 267.3 ± 4.8 mg g⁻¹ (*n* = 4) (Al-Negheimish et al., 2021; Alsheyab and Khedaywi, 2016; Laforest and Duchesne, 2006; Li et al., 2023; Loaiza et al., 2017; Stathopoulos et al., 2013; Xia and Picklesi, 2000); in contrast, some previous studies also found the average or median Fe content to be around 400–500 mg g⁻¹ (Machado et al., 2006; Patil et al., 2013; Ye et al., 2021), slightly higher than our results.

Despite some variability in Fe content reported by our and previous studies (Table S6), the mean or median Fe content are generally around 300–500 mg g⁻¹ for steelwork fly ash. In a recent modeling study (Rathod et al., 2020), the Fe content in steelwork fly ash was set to 440 mg g⁻¹ (and the lower and upper bounds were set to 150 and 950 mg g⁻¹), being consistent with experimental results.

3.1.4 Biofuel burning aerosol

Our work considered biofuel burning aerosols for nine types of biofuels, including four types of crop straw, one type of wild grass, and four types of wood. Fe content in biofuel burning aerosols ranged from 0.002 to 0.101 mg g⁻¹ (Table 2), with average and median values being 0.023 ± 0.026 and 0.013 mg g⁻¹, respectively. As shown in Table S6, the average Fe content was determined to be 0.024 ± 0.017 mg g⁻¹ (*n* = 3) for PM_{2.5} (Patil et al., 2013), very close to our result; in another study (Hildemann et al., 1991), it was determined to be 0.090 mg g⁻¹ for PM₂ (*n* = 2), higher than our result. In some other studies, average Fe content were reported to be in the range of 0.162–0.440 mg g⁻¹ for PM_{2.5} (Alves et al., 2011; Hedberg et al., 2002; Watson et al., 2001; Zhang et al., 2012) and 0.723 ± 0.661 mg g⁻¹ for PM₁₀ (Schmidl et al., 2008), much higher than our results.

Fe content in biofuel burning aerosols showed large variability in different studies, likely due to variations in combustion conditions and biofuel types. For example, metal content in biofuel burning aerosols depended greatly on biofuel types and regions where biofuel was collected (Goncalves et al., 2010), and aerosol particles emitted by wild grass combustion contained larger amounts of metal than wood combustion (Jahn et al., 2021). Modeling studies have used a similar distribution of Fe content between 0.2 and 0.580 mg g⁻¹

for biofuel burning aerosols (Luo et al., 2008; Rathod et al., 2020).

3.1.5 Fe contents: comparison of anthropogenic and dust Fe

Figure 3a displays Fe content for anthropogenic particles examined in our current study, and the brown dashed line represents the average Fe content of desert dust (35 mg g⁻¹) (Taylor and McLennan, 1995). Steelwork fly ash has very high Fe content (median: 346.5 mg g⁻¹), about one order of magnitude higher than desert dust. Power plant coal fly ash (median: 35.0 mg g⁻¹) has similar Fe content to desert dust. Compared to desert dust, Fe content were around three orders of magnitude lower for residential coal and biofuel burning aerosol (median: 0.038 and 0.013 mg g⁻¹, respectively). The Fe content was much lower for residential coal and biofuel burning aerosol, likely due to lower combustion temperatures. When combustion occurs at lower temperature, the carbon content of emitted particles is higher; in addition, lower combustion temperature is not sufficient to enable Fe in the fuel to enter emitted particles via volatilization-condensation processes.

3.2 Fe solubility by fuel type

3.2.1 Power plant coal fly ash

Fe solubility in acetate buffer (pH: 4.3) ranged from 0.002 % to 0.17 % for power plant coal fly ash (Table 2), with the average and median values being 0.05 ± 0.05 % and 0.03 %, respectively. A few previous studies measured Fe solubility of power plant coal fly ash in weakly acidic or circumneutral solutions (Table S7). For example, Fe solubility was measured to be 0.06 % in deionized water (Oakes et al., 2012), similar to our result; it was measured to be 0.2 % in dilute sulfuric acid solution (pH: 4.7) (Desboeufs et al., 2005), slightly higher than our result; the median Fe solubility was determined to be 0.13 % in acetate buffer (pH: 4.3) and 0.06 % in deionized water (Li et al., 2022b), both higher than the median value we obtained. Overall, our work and previous studies suggest that Fe solubility is low in weakly acidic and circumneutral solutions for power plant coal fly ash, with mean or median values around 0.1 %.

Some studies also measured Fe solubility of power plant coal fly ash in highly acidic solutions and found them to be much higher than those in weakly acidic and circumneutral solutions. For example, Fe solubilities were found to be in the range of 20 %–25 % at pH of 1–2 (Chen et al., 2012), 4.2 %–8.3 % at pH of 2 (Fu et al., 2012), and > 40 % at pH of 2.1 (Baldo et al., 2022). Although Fe solubility measured in strongly acidic solutions may not reflect initial Fe solubility, these studies suggested that acid processing in the emission plume or wider atmosphere could greatly increase Fe solubility for power plant coal fly ash.

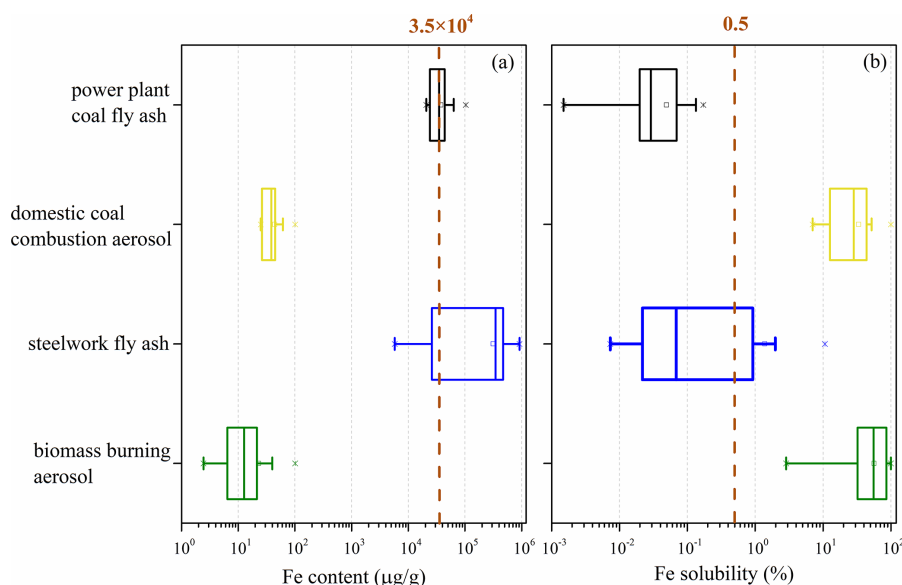


Figure 3. Fe content (a) and solubility (b) measured in our work for power plant coal fly ash, residential coal combustion aerosol, steelwork fly ash, biofuel burning aerosol, municipal waste fly ash and oil fly ash. The two brown dash lines represent (a) the Fe content ($3.5 \times 10^4 \mu\text{g g}^{-1}$) and (b) Fe solubility ($\sim 0.5\%$) for desert dust, respectively.

3.2.2 Residential coal combustion aerosol

Fe solubility in acetate buffer (pH: 4.3) was determined to range from 7.03 % to 100 % for residential coal combustion aerosol (Table 2), with the average and median values being $33.30 \pm 27.71\%$ and 28.45 %, respectively. To our knowledge, no previous study has measured Fe solubility for residential coal combustion aerosol. Compared to power plant coal fly ash, Fe solubility was much higher for residential coal combustion aerosol, and such difference can be attributed to much higher temperature in power plant coal combustion than residential coal combustion. Pyrite (FeS_2) is the major Fe-containing mineral in coal (Deng et al., 2015; Oliveira et al., 2016; Rathod et al., 2020). In low-temperature combustion, pyrite is mainly transformed to Fe sulfate (Bhargava et al., 2009) which has very high Fe solubility; as the temperature increases to $> 1000\text{ K}$, Fe sulfate is further transformed to hematite and magnetite which exhibit very low solubility (Hu et al., 2006; Ram et al., 1995; Rathod et al., 2020). A previous study (Rathod et al., 2020) used the relationship between combustion temperature and Fe mineralogy in emitted particles to estimate Fe solubility for different combustion aerosols, and Fe solubility was estimated to be as high as $\sim 32.5\%$ for residential coal combustion aerosols, in good agreement with our experimental results.

3.2.3 Steelwork fly ash

Fe solubility in acetate buffer (pH: 4.3) was determined to range from 0.01 % to 10.64 % for steelwork fly ash (Table 2), and the average and median values were $1.37 \pm 2.77\%$ and 0.07 %, respectively. We note that Fe solubility was signif-

icantly higher (0.92 %–8.59 %) for 8 samples and very low ($< 0.5\%$) for the other 21 samples (Table S3), most of which showed Fe solubility below 0.1 %. No previous work has measured Fe solubility for steelwork fly ash. Our experimental results were supported by a modeling study (Rathod et al., 2020) which suggested that the major Fe-containing species in steelwork fly ash were Fe oxides with very low Fe solubilities.

3.2.4 Biofuel burning aerosol

For biofuel burning aerosol, Fe solubility in acetate buffer (pH: 4.3) ranges from 2.86 % to 100 % with average and median values of $56.07 \pm 30.95\%$ and 55.87 %, respectively (Table 2). Based on the relationship between combustion temperature and Fe-containing species in emitted aerosols, Fe solubility was previously estimated at 35 % for wood burning (i.e., biofuel) aerosol (Rathod et al., 2020), in good agreement with our experimental results.

The biofuel examined in our experiment was burnt in a sealed stove and contained no apparent local soil contamination. As such, these results are most representative of domestic biofuel combustion for which the influence of soil-derived Fe can be expected to be negligible. In contrast, wildfires represent dynamic open fire systems that emit aerosol Fe in both fine and coarse fractions (Hamilton et al., 2019). During wildfire combustion, not only is the biofuel (biomass) consumed, but local soils are also entrained into the smoke plumes (Hamilton et al., 2022; Tegler et al., 2023). These soil-derived particles are typically larger (in particle size) and less soluble than their biofuel-derived counterparts (Hamil-

ton et al., 2022), resulting in a larger mass of emitted Fe, albeit with a lower overall Fe solubility. Future studies would benefit from capturing emissions from open burning scenarios to better characterize the properties of wildfire-emitted Fe.

3.2.5 Fe solubilities: comparison of anthropogenic and dust Fe

Figure 3b compares our measured Fe solubility for four types of combustion and anthropogenic particles with that for desert dust. Biofuel burning aerosols (median: 55.87 %) and residential coal combustion aerosols (median: 28.45 %) exhibited very high Fe solubility. Compared to desert dust, for which Fe solubility is around 0.5 % (Chuang et al., 2005; Li et al., 2022b; Ooki et al., 2009; Schroth et al., 2009; Shi et al., 2011), Fe solubility was lower for steelwork fly ash (median: 0.07 %) and power plant coal fly ash (median: 0.03 %).

Overall, Fe solubility in emitted particles was significantly higher for low-temperature combustion (residential and biofuel burning aerosols) than high-temperature combustion (steelwork fly ash and power plant coal fly ash). This is because Fe in emitted particles is mainly highly soluble Fe sulfates for low temperature combustion (Bhargava et al., 2009; Rathod et al., 2020) but Fe oxides with very low solubility for high temperature combustion (Hu et al., 2006; Ram et al., 1995; Rathod et al., 2020).

3.3 Modeling Results

Leveraging new measurements of combustion Fe solubility in residential fuel sources as reported in Sect. 3.1 and 3.2, we performed a series of Earth System Model (MIMI) simulations that examined global Fe fluxes in response to modifying anthropogenic Fe solubility parameters at their point of emission. To pair observed solubilities (Table 2) with fuel-types represented in the model, we updated Fe solubility in residential coal burning aerosol from 0.2 % to 33 % and in biofuel burning aerosol from 10 % to 56 % at the point of emission (Table 3) in both the fine and coarse modes. Biofuel Fe emissions are not limited to residential sources in our Fe inventory. However, lacking updated measurements for industrial biofuel combustion sources, the newly derived solubility parameter (56 %) was applied uniformly within the “BIOF” grouping. Waste Fe solubility was added for the central- simulations and was set to 1.5 %, following new experimental results provided in Table S7. Smelting Fe solubility was kept at 0.03 % for all simulations, since new data did not suggest an alternative solubility from what is currently used (Table 3). We ran one additional simulation with updates to industrial sources (PD-IND: industrial coal Fe solubility from 0.2 % to 0.05 % and oil from 38 % to 25 %), but observed impacts to global soluble Fe fluxes following these changes were minimal and are accordingly deferred to the Supplement. A description of the fractional solubilities applied to each anthro-

pogenic fuel type within each model simulation is provided in Table 3.

3.3.1 Impacts on global soluble Fe distribution

By applying two new emissions inventories and new solubility parameters for residential Fe emissions within MIMI, we report a new range of soluble Fe fluxes to the ocean with regional variations. To isolate the impacts of modifications to each fuel-source, we compared each model case. When comparing PD-BASE to PD-RESI, the emissions inventory had a greater influence on the result rather than solubility parameters, per sizeable differences in residential coal emissions by mass. In the high-residential inventory, global Fe emissions from residential coal were 460 Gg a^{-1} , exceeding individual emissions from all other fuel types (industrial coal: 310 Gg a^{-1} ; oil: 34 Gg a^{-1} ; biofuel: 72 Gg a^{-1}) except for smelting (1350 Gg a^{-1} ; Table S8). Whereas, in the central-residential inventory, emissions were two orders of magnitude less at 4.9 Gg a^{-1} (Table S9), and residential coal sources were the second lowest contributor to total anthropogenic Fe emissions, next to waste (0.9 Gg a^{-1}). Constraining the Fe content in residential emissions is therefore a more critical knowledge gap to be addressed than constraining the fractional solubility of this source.

Accordingly, when applying the central-residential emissions inventory and using the PD-RESI solubility parameters, soluble Fe fluxes to the global ocean only increased by $< 1 \text{ Gg a}^{-1}$ (Fig. 4; Table 4). Conversely, when applying the high-residential inventory, we saw a 92 % increase in anthropogenic soluble Fe fluxes ($+33 \text{ Gg a}^{-1}$) to the ocean, translating to a 7 % increase in overall soluble Fe fluxes including those from dust and wildfire (Fig. 4; Table 4). While the high-residential emissions inventory likely overstates residential coal burning emissions by Fe mass content, the ocean regions most influenced by residential coal burning become apparent, facilitating future research locations of highest interest. Anthropogenic soluble Fe delivery to the Indian Ocean, eastern North Pacific, and parts of the Southern Ocean increased by 300 % to 400 %, corresponding with a large increase in emissions from China, India, Australia, and South Africa (Fig. 4). This follows previous reports of relatively large anthropogenic signals from these regions when compared to global averages (Rathod et al., 2024; Wang et al., 2015).

Despite large differences in residential coal emissions between our high- and central-residential inventories, biofuel emissions by mass were nearly identical between inventories (72 and 71 Gg a^{-1} , respectively) because wood burning was already an isolated fuel source in our inventory (Rathod et al., 2020). The small difference is introduced by the separation of waste as a distinct source in the central-residential inventory. When using the high-residential inventory, impacts to soluble Fe fluxes by biofuel were largely overshadowed by residential coal, but using the central- inventory, changes to biofuel

Table 3. Fractional Fe solubilities applied in each model simulation to reflect experimental findings. Bolded rows indicate baseline simulations with no changes made to Fe solubility from previous work using MIMI. To underscore modifications between simulations, a dash (–) is provided where assigned solubility did not differ from the PD-BASE simulation.

Simulation	Fe solubility modifications by fuel-type (%)					
	Industrial Coal	Residential Coal	Oil	Biofuel	Smelting	Waste*
PD-BASE	0.2	0.2	38	10	0.003	1.5
PD-RESI	–	33	–	–	–	–
PD-BIOF	–	33	–	56	–	–
PD-IND	0.05	33	25	56	–	–
PI-BASE	NA	NA	NA	10	NA	NA
PI-BIOF	NA	NA	NA	56	NA	NA
MID-SSP370-BASE	0.2	0.2	38	10	0.003	NA
MID-SSP370-BIOF	–	33	–	56	0.003	NA
END-SSP370-BASE	0.2	0.2	38	10	0.003	NA
END-SSP370-BIOF	–	33	–	56	0.003	NA

* Only applied in the central-residential simulations.

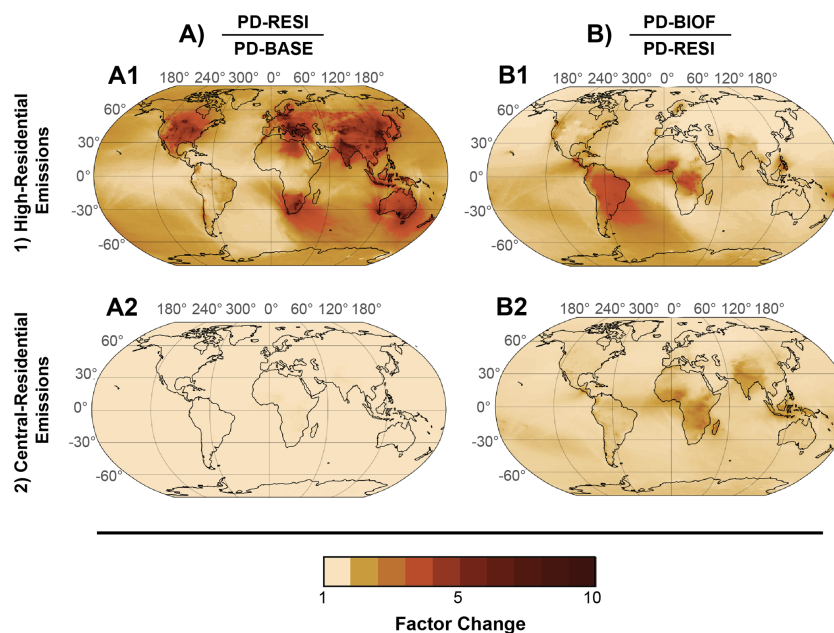


Figure 4. Relative changes to soluble Fe deposition fluxes using different (1–2) emission inventories and following modifications to (A–B) Fe solubility parameters.

parameters in the model controlled increases in soluble Fe fluxes. When we increased biofuel Fe solubility (PD-BIOF), soluble Fe fluxes to the ocean increased by an additional 11 Gg a^{-1} , for a total increase of $< 1\text{--}44 \text{ Gg a}^{-1}$ from residential sources (residential coal + biofuel) when compared to PD-BASE (Table 5). Changes to soluble Fe fluxes from biofuel burning were most concentrated across the South Atlantic (Fig. 4), likely due to the long range transport of emissions from the Amazon rainforest and across the Congo River basin where biofuel-burning in cook stoves is a com-

mon residential practice (García-López et al., 2025; Stoner et al., 2021). It is notable that the signal from central and sub-Saharan Africa impacting the equatorial Atlantic is pronounced using both inventories, but the signal from South America impacting the South Atlantic was much weaker for the central inventory. We report a maximum change in soluble Fe fluxes using the high-residential emissions inventory and PD-BIOF solubility parameters, with deposition to the ocean doubling from 36 to between 49–81 Gg a^{-1} at the global scale (relative to PD-BASE; Table 5).

Table 4. Global present day soluble Fe deposition fluxes in Gg a^{-1} (relative contribution in %) to the ocean for dust, wildfire, and anthropogenic combustion sources. Ranges reflect deposition fluxes between the central- and high-residential emissions inventories (only when variable between cases). Regional fluxes are reported in the Supplement (Tables S10–S12).

Model Simulation (case)	Dust	Wildfire	Anthropogenic Combustion	All Sources
PD-BASE	305 (83 %)	26 (7 %)	36 (10 %)	367 (100 %)
PD-RESI	305 (76 %–83 %)	26 (7 %)	37–70 (10 %–17 %)	368–401 (100 %)
PD-BIOF	305 (74 %–81 %)	26 (6 %–7 %)	49–81 (12 %–20 %)	375–412 (100 %)

Table 5. Global anthropogenic combustion Fe emission and deposition fluxes (Gg a^{-1}) in the preindustrial (PI), present day (PD), and Future (FU), as simulated by MIMI to two significant figures. Where ranges are reported reflect use of the central-/high-residential emissions inventories.

Emission Scenario	Model Simulation (case)	Fe Content	Global Emission	Global Deposition	Deposition to Ocean
PI (1750 CE)	PI-BASE	Total (Soluble)	0.80 (0.08)	0.80 (0.10)	0.30 (0.04)
	PI-BIOF	Total (Soluble)	0.80 (0.44)	0.80 (0.50)	0.30 (0.20)
PD (2010 CE)	PD-BASE	Total (Soluble)	2220 (20–21)	2220 (89–90)	590 (36–40)
	PD-BIOF	Total (Soluble)	2220 (56–170)	2220 (121–270)	590 (46–81)
FU (2050 CE)	MID-SSP370-BASE	Total (Soluble)	2400 (20)	2400 (90)	620 (40)
	MID-SSP370-BIOF	Total (Soluble)	2400 (180)	2400 (250)	620 (80)
FU (2100 CE)	END-SSP370-BASE	Total (Soluble)	1970 (20)	1970 (80)	510 (30)
	END-SSP370-BIOF	Total (Soluble)	1970 (90)	1970 (150)	510 (50)

With soluble dust-Fe (310 Gg a^{-1}) and wildfire-Fe (30 Gg a^{-1}) fluxes, our different anthropogenic cases (an additional $13\text{--}45 \text{ Gg a}^{-1}$; Table 5) suggest that total soluble Fe fluxes to the ocean fall between 370 Gg a^{-1} (PD-BASE) and $380\text{--}410 \text{ Gg a}^{-1}$ (PD-BIOF) at the global scale. These values fall within previous ranges of uncertainty as reported for Fe deposition fluxes to the ocean (Hamilton et al., 2023; Ito and Miyakawa, 2023), suggesting that solubility modifications tested herein align with previous Fe constraints within Earth System Models.

3.3.2 Model-observation comparisons of total and soluble Fe concentrations

Comparison of modeled surface concentrations with regionally grouped, ship-based observations revealed generally good agreement between modeled and observed total and soluble aerosol Fe concentrations for all PD simula-

tions (Fig. 5). Modeled total Fe concentrations were slightly underpredicted when compared to observed values but remained well within one order of magnitude for each ocean region, with the exception of the Southern Ocean where total Fe was underestimated by several orders of magnitude. This aligns with previous efforts to model global fluxes of total and soluble aerosol Fe using MIMI v1.0 and other Earth System Models (Ito and Miyakawa, 2023; Ito et al., 2019; Liu et al., 2024). Current hypotheses suggest that an Fe source, such as volcanism or mining, is not currently well represented in models, or alternatively, that limited observations are not representative of Fe conditions in the airshed of the Southern Ocean (Ito and Miyakawa, 2023; Liu et al., 2024).

In each case, soluble Fe regression analyses followed a similar trend to total Fe, wherein modeled averages were slightly lower than observed values and fell within one order of magnitude, apart from the Southern Ocean and Ara-

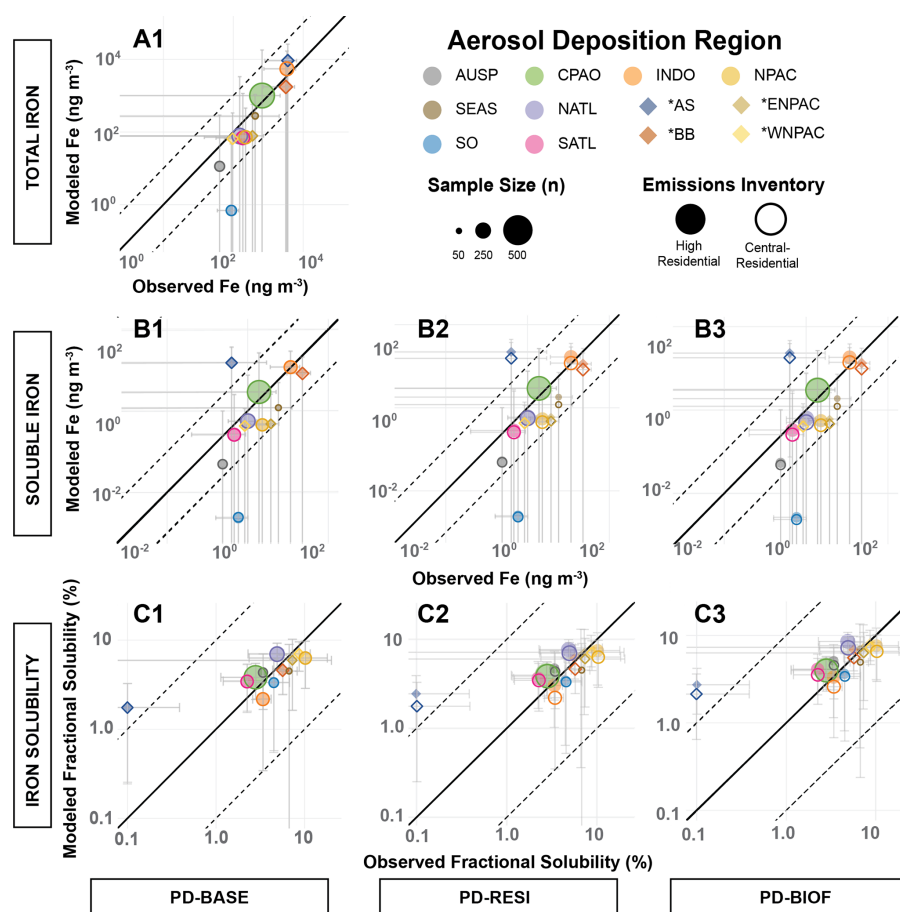


Figure 5. Comparison of modelling and observational data: (A) total Fe, (B) soluble Fe, and (C) Fe solubility; (1) PD-BASE, (2) PD-RESI, and (3) PD-BIOF. Data were aggregated over time and space as medians. Solid/hollow markers indicate use of the high/central-residential emissions inventories, respectively. Error bars represent spatiotemporal variance within each region. The solid black line indicates a 1-to-1 relationship and the dashed lines represent deviation by ± 1 order of magnitude. Only PD-BASE is shown for total Fe per consistency between cases.

bian Sea (Fig. 5, Tables S14–S15). In the PD-RESI and PD-BIOF cases, soluble Fe concentrations increased at the global scale, but the degree varied by region. At the global scale, enhancing residential Fe emissions generally improved model skill for soluble Fe concentrations (Fig. 5), resulting in an average increase to modeled soluble Fe concentrations by $0.5 \pm 0.7 \text{ ng m}^{-3}$ within each ocean region (Tables S14–S15). For regions most influenced by residential coal burning, the improvement in model skill was slightly higher using the high-emissions inventory, especially for Southeastern Asia ($\Delta\text{RMSE} = -0.4$), the Bay of Bengal ($\Delta\text{RMSE} = -4.7$), and the eastern North Pacific (Fig. 5; Tables S14–S15; $\Delta\text{RMSE} = -0.1$). For biofuel burning Fe, the emissions inventory had less of an impact, but enhancing Fe solubility most improved model skill within the South Atlantic Ocean (Fig. 5, Tables S14–S15, $\Delta\text{RMSE} = -0.05$). Complete summary statistics conveying impacts to model skill for soluble Fe concentrations simulated in each run are provided in the Supplement (Tables S14–S15).

While the high-residential emissions inventory slightly improved estimates for soluble Fe concentrations, the central-residential emissions inventory performed better when capturing fractional solubility for regions influenced by residential coal (Fig. 5). Despite these noticeable variations between cases, ultimately, Fe solubilities calculated by the model were aligned with observations within ± 1 order of magnitude for every region except for the Arabian Sea wherein solubility was overestimated by 1–2 orders of magnitude (Fig. 5). In previous MIMI-validation efforts (Hamilton et al., 2019), observational data from the Arabian Sea and Bay of Bengal were aggregated as the Indian Ocean and this result was not flagged. While both basins receive substantial anthropogenic aerosol from India, dust from the Middle East more strongly influences the Arabian Sea, and the Bay of Bengal is more strongly affected by anthropogenic emissions across Southeastern Asia (Bali et al., 2019; Guieu et al., 2019).

In general, we found that regions with higher dust inputs more often overshoot measurements when compared to regions with less dust deposition and higher relative impact by anthropogenic emissions (Fig. 5; Tables S14–S15). In each of our modified solubility cases (PD-RESI and PD-BIOF), Fe solubility for southeastern Asia, the Bay of Bengal, and the North Pacific increased, but the regions heavily impacted by dust remained relatively unchanged (Fig. 5).

Withstanding source-apportioned measurements of residential coal or biofuel aerosol in our observational dataset, we performed additional model-observation comparisons only using measurements collected in ocean regions downwind of strong residential burning influences. These regions were defined as model-resolution grid cells wherein soluble Fe fluxes increased by 100 % or more in the PD-BIOF simulations (Fig. 4). However, this reduced median-aggregated observational data points from $n = 990$ to $n = 25$, limiting statistical capacity to constrain model fluxes. When using the smaller observational dataset, model-observational comparisons for total Fe, soluble Fe, and solubility mirrored agreement trends using the larger dataset (Fig. 5); those regression analyses are provided in the Supplement (Figs. S6–S7) with results from the PD-IND simulation.

Anthropogenic soluble Fe fluxes to marine ecosystems increased by 28 % to 123 % (2 % to 10 % total Fe) when considering all sources of Fe, including dust and biomass burning using the PD-BIOF solubility parameters. For some ocean regions, the increase in soluble Fe fluxes exceeded 150 % when using the high-emissions inventory. Despite this, changes to model skill were ultimately modest (Fig. 5). The sizeable changes in fluxes with minimal changes to model skill further reinforce the current limitations of ship-based observations in capturing representative soluble Fe fluxes, particularly in the under-sampled Southern Hemisphere and in regions influenced by residential coal and biofuel burning. Future efforts should prioritize expanding the spatial coverage of measurements in these regions to improve model accuracy and understanding of possible anthropogenic influence on remote marine biogeochemistry.

3.3.3 Soluble Fe under PI and FU emission scenarios

PI model simulations serve as a valuable reference point in understanding the specific implications of anthropogenic perturbation to the Earth system. For most regions, soluble Fe fluxes increased between the PI and PD eras (Fig. 6), largely attributed to steadily growing anthropogenic combustion emissions and industrial activities over time. Dust and wildfire Fe emissions were also distinct between the PI and PD, due to climatic and land-use change induced feedbacks that have altered global precipitation patterns and dust suspension (Hamilton et al., 2018; Kok et al., 2023; Li et al., 2019; Mahowald et al., 2010). At the global scale, we estimated that current soluble Fe fluxes to marine ecosystems exceed PI fluxes by 36–70 Gg a⁻¹, apart from the South

Atlantic, wherein soluble Fe fluxes have decreased since the PI era by 2.8–5.6 Gg a⁻¹ (Fig. 6). This decrease was likely attributed to reduction in wildfire burned area over past decades, particularly in sub-Saharan Africa (Andela et al., 2017; Jones et al., 2022). Previous work has suggested that wildfire activity during the PI era exceeded current wildfire regimes at the global scale (Hamilton et al., 2018).

Regardless of the inventory applied, we observed the largest increases between PI and PD soluble Fe fluxes in Southeastern Asia, the Bay of Bengal, and the North Atlantic. In Southeastern Asia anthropogenic activity has specifically driven, and is projected to drive, changes to future soluble Fe fluxes (Fig. 6). This was the only ocean region wherein anthropogenic sources were comparable (central-residential inventory) or exceeded (high-residential inventory) dust sources of soluble Fe (Fig. 6). When using the high-residential inventory and the -BIOF solubility parameters, anthropogenic combustion aerosol constituted between 55 %–72 % of soluble Fe fluxes to marine ecosystems in Southeastern Asia, up to a 21 % increase from PD-BASE, i.e., based on model solubility parameterizations. Although dust was still the largest source of Fe to the Bay of Bengal and North Atlantic, anthropogenic combustion also strongly influenced soluble Fe delivery in these regions (Fig. 6). When using the high-residential emissions inventory with the -BIOF solubility parameters, the relative contribution by anthropogenic emissions doubled in these regions (Tables S10–S12).

The inventory and solubility parameters used in each case revealed important implications for projected trends of soluble Fe fluxes moving into the second half of the 21st century. Under the SSP370 FU emissions scenario, anthropogenic Fe fluxes were projected to reach their maxima by 2050 for most deposition regions and then decrease to values at or below current PD conditions by 2100 (Fig. 6). However, this trend did not hold for regions within the Southern Hemisphere (Australia/South Pacific, Central Pacific/Atlantic, and Southern Ocean) where soluble aerosol Fe fluxes were projected to continually increase through the end of the century (Fig. 6). This was not due to direct changes in anthropogenic combustion emissions, but rather due to changes in dust emissions as the primary source of soluble Fe to the Southern Hemisphere (Fig. 6).

By the end of the century under SSP370, PD-BASE simulations suggest that soluble Fe deposition to global marine systems will increase slightly from 367 to 369 Gg a⁻¹ (~ 1 % increase) by 2100. However, when considering higher residential Fe emissions with higher solubilities representing new upper bound, projected changes to soluble Fe fluxes between PD/MID-SSP370 and MID-SSP370/END-SSP370 was reversed at the global scale and for many regions, with projected decreases by the end of the century (~ 2 % decrease; Fig. 6). The projected losses in soluble Fe between the middle and end of the 21st century was especially apparent for the Bay of Bengal (2 %–6 %), the eastern and west-

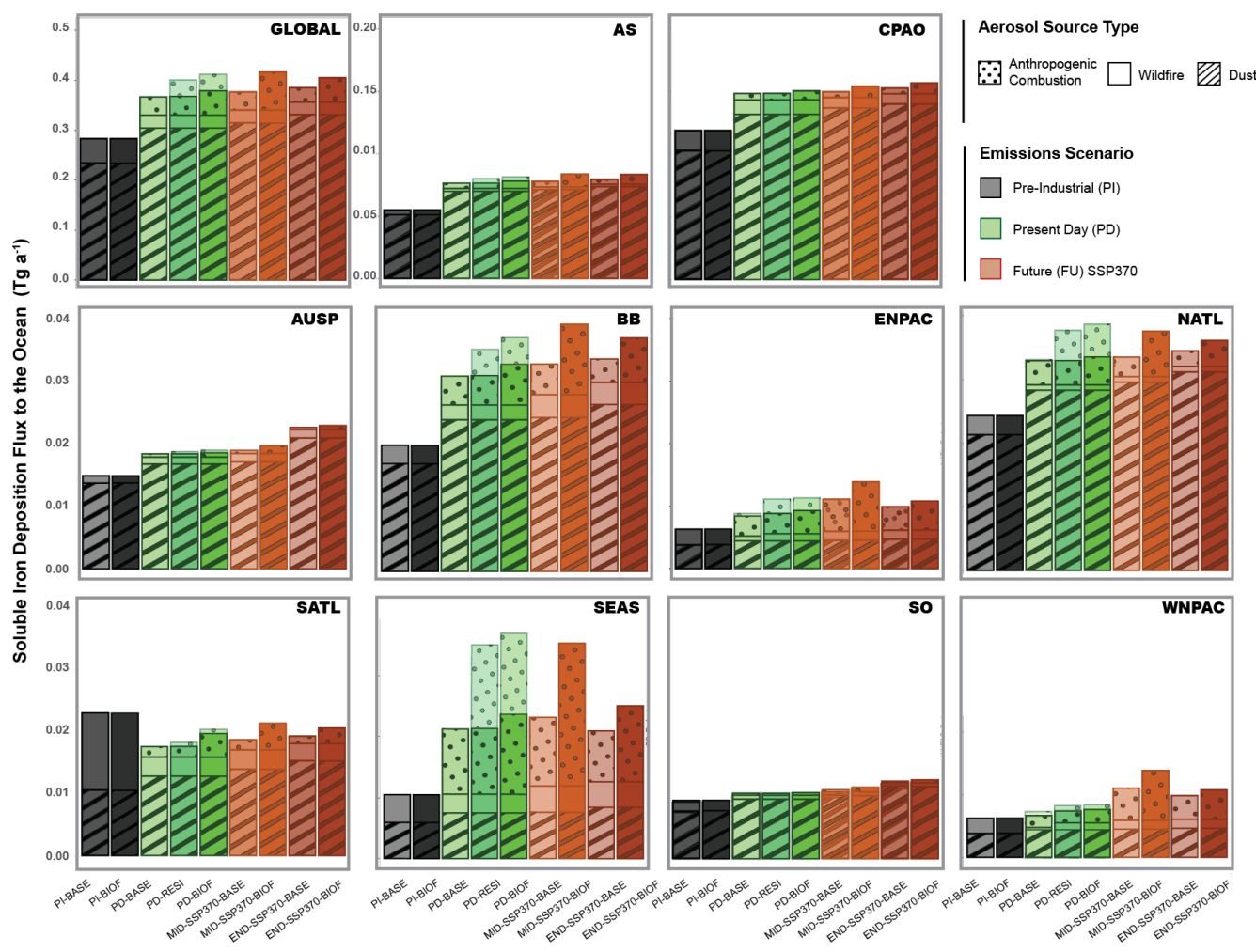


Figure 6. Deposition fluxes of soluble aerosol Fe to marine ecosystems at the global and regional scale. Deposition fluxes are source-apportioned (dust, wildfire burning, and anthropogenic combustion) and provided for each case with distinct solubility parameters. For the PD, transparent bars represent the high-residential emissions inventory and opaque represent the central-. Conversely, for the FU, only the high-residential inventory was applied, and the bars are opaque.

ern North Pacific (12%–29%), and across Southeastern Asia (11%–41%) (Fig. 6), suggesting that various marine ecosystems could face a more significant deviation from current soluble Fe supply than has previously been represented in Earth System Models.

Projected changes in soluble Fe fluxes by 2100 under FU emission scenarios, including SSP370, have strong implications for the spatiotemporal distribution of net marine primary productivity, mostly in Fe limited regions. For example, although we demonstrated that anthropogenic emissions most greatly influenced Fe dynamics across Southeastern Asia, it is important to note that primary production in this ocean region is not typically limited by Fe (Bazzani et al., 2023), so ecosystem-level effects by atmospheric Fe are less likely to be observed therein. However, similar to Southeastern Asia, we found that changes to anthropogenic emissions more strongly impacted soluble Fe fluxes in the eastern North

Pacific when compared to dust and wildfire sources. Recent work suggests that the atmospheric supply of anthropogenic Fe has already shifted phytoplankton bloom dynamics in the open ocean by accelerating the seasonal uptake of upwelled nitrogen in HNLC regions, including North Pacific (Hawco et al., 2025). Such regions are anticipated to be especially sensitive to changes in anthropogenic Fe given that they are historically limited by trace metals including Fe (Bazzani et al., 2023; Moore et al., 2013; Nishioka and Obata, 2017).

In addition to our findings, diverse lines of evidence suggest that half of the soluble Fe flux to the North Pacific comes from Asian anthropogenic sources (Hamilton et al., 2019, 2020a; Hawco et al., 2025; Rathod et al., 2020). Li et al. (2024) found that the magnitude of chlorophyll-a response to Fe deposition off the coast of China was lowered by a factor of 4 during COVID-19 in March 2020 when anthropogenic emissions across East Asia were substantially reduced. The

authors speculated that a reduction in soluble Fe from anthropogenic activities, either via the primary emission of soluble Fe or via a reduction in Fe solubilization via co-emitted acidic species (e.g., SO_x), resulted in a lessened supply of soluble Fe delivered during the deposition event. Moreover, using Fe isotopes to trace source origins of atmospheric Fe, Hawco et al. (2025) recently showed that the springtime delivery of anthropogenic Fe could be one major factor driving observed seasonal and geographic shifts to the North Pacific transition zone, a highly productive boundary in the North Pacific. Isotopic signatures capable of distinguishing residential coal combustion from other anthropogenic combustion sources have not yet been identified, but our findings suggest that residential coal burning is an especially important source of soluble Fe to the North Pacific and the South China Sea, and across southeastern Asia. Accordingly, we find that projected losses of anthropogenic emissions over the course of this century will most greatly influence nutrient dynamics in these key marine ecosystems.

4 Conclusions

Anthropogenic activity has added a multitude of new aerosol Fe sources to the atmosphere. Understanding how these new sources alter the magnitude and timing of soluble Fe aerosol fluxes to the ocean aids understanding of how human activity is changing marine primary productivity and ocean ecosystem functions within the Anthropocene. However, estimating the contribution of anthropogenic emissions to soluble aerosol Fe fluxes is challenging given the wide variety of sources, each with their own distinct physicochemical profiles. Lack of observational constraints leads to large variation across different modeling studies on the magnitude of the deposition flux from anthropogenic sources. We address some of these uncertainties in this study by measuring the Fe content and solubility of aerosol Fe from several important anthropogenic sources, including a first assessment of the contribution from two major biofuels, namely residential coal and wood. We find that median Fe solubilities vary by greater than three orders of magnitude across fuel types, from 0.03 % for power plant coal fly ash to 55.87 % for biofuel burning aerosol.

To understand the impact of increasing anthropogenic source representations of fractional Fe solubility, we created three new emission inventories that distinguished residential from industrial sources, and further refined Fe solubility parameters for each source within MIMI, an atmospheric Fe module embedded within the CESM2.

At the global scale, we found that current (PD) soluble Fe fluxes to the ocean from anthropogenic sources could exceed current modeled values by somewhere between 28 % and 123 %. This represents a potential increase of over 3 orders of magnitude from the PI when biofuel sources are assumed to be the only source of anthropogenic Fe (Hamilton

et al. 2020a). Projected (FU) soluble Fe fluxes from anthropogenic sources remain similar to the PD through to the middle of the century before declining by up to 38 % at the end of the century under SSP370.

At the regional scale, including residential coal and biofuel burning sources in the model resulted in the most notable impacts for the Bay of Bengal, across Southeast Asia, and throughout the North Pacific and North Atlantic (i.e., regions strongly influenced by nearby continental anthropogenic activity). However, these regions are generally under-sampled in terms of shipborne aerosol Fe observations, and therefore, to reduce the largest source of uncertainty, more measurements are needed in regions downwind of residential Fe sources to better constrain the contribution of human activity on global biogeochemical cycles.

Code and data availability. Experimental data can be found in the manuscript or the Supplement, or are available at <https://doi.org/10.5281/zenodo.17766592> (Li, 2025). Modeling output data, coding scripts and emission inventories are available at <https://doi.org/10.5281/zenodo.17903186> (Hamilton and Plaas, 2025).

Supplement. The supplement related to this article is available online at <https://doi.org/10.5194/acp-26-9037-2026-supplement>.

Author contributions. MT initiated this study; MT and DSH designed this study and secured funding resources; RL, YZ, YC and TZ conducted experimental work; HEP, SR and DSH conducted modeling work; YY provided key samples used in this work and contributed to data analysis; RL and HEP analyzed the results; RL, HEP, DSH and MT wrote the manuscript; all the authors reviewed and approved the manuscript.

Competing interests. At least one of the (co-)authors is a member of the editorial board of *Atmospheric Chemistry and Physics*. The peer-review process was guided by an independent editor, and the authors also have no other competing interests to declare.

Disclaimer. Publisher's note: Copernicus Publications remains neutral with regard to jurisdictional claims made in the text, published maps, institutional affiliations, or any other geographical representation in this paper. The authors bear the ultimate responsibility for providing appropriate place names. Views expressed in the text are those of the authors and do not necessarily reflect the views of the publisher.

Special issue statement. This article is part of the special issue "RUSTED: Reducing Uncertainty in Soluble aerosol Trace Element Deposition (AMT/ACP/AR/BG inter-journal SI)". It is not associated with a conference.

Financial support. This work was sponsored by National Natural Science Foundation of China (grant nos. 42321003, 42507154, and 42277088), International Partnership Program of Chinese Academy of Sciences (grant no. 164GJHZ2024011FN), and Guangzhou Bureau of Science and Technology (grant no. 2024A04J6533). This work was partially supported from funding to SCOR WG 167 (RUSTED) provided by national committees of the Scientific Committee on Oceanic Research (SCOR) and from a grant to SCOR from the U.S. National Science Foundation (grant no. OCE-2513154).

Review statement. This paper was edited by Qiang Zhang and reviewed by Akinori Ito, Weijun Li, and one anonymous referee.

References

- Ahmaruzzaman, M.: A review on the utilization of fly ash, *Prog. Energ. Combust.*, 36, 327–363, <https://doi.org/10.1016/j.peccs.2009.11.003>, 2010.
- Al-Abadleh, H. A., Kubicki, J. D., and Meskhidze, N.: A perspective on iron (Fe) in the atmosphere: air quality, climate, and the ocean, *Environ. Sci.-Proc. Imp.*, 25, 151–164, <https://doi.org/10.1039/D2EM00176D>, 2023.
- Alizadeh, M. and Momeni, M.: The effect of the scrap/DRI ratio on the specification of the EAF dust and its influence on mechanical properties of the concrete treated by its dust, *Constr. Build. Mater.*, 112, 1041–1045, <https://doi.org/10.1016/j.conbuildmat.2016.03.011>, 2016.
- Al-Negheimish, A. I., Al-Mutlaq, F. M., Fares, G., Alhozaimy, A. M., and Iqbal Khan, M.: Characterization of chemical accelerators for sustainable recycling of fresh electric-arc furnace dust in cement pastes, *Adv. Powder Technol.*, 32, 3046–3062, <https://doi.org/10.1016/j.apt.2021.06.019>, 2021.
- Alsheyab, M. A. T. and Khedaywi, T. S.: Analysis of the Effect of Temperature on the Resilient Modulus of Asphalt Concrete Mixed with Electric Arc Furnace Dust (EAFD), *Water Air Soil Poll.*, 227, 80, <https://doi.org/10.1007/s11270-016-2776-4>, 2016.
- Alves, C., Gonçalves, C., Fernandes, A. P., Tarelho, L., and Pio, C.: Fireplace and woodstove fine particle emissions from combustion of western Mediterranean wood types, *Atmos. Res.*, 101, 692–700, <https://doi.org/10.1016/j.atmosres.2011.04.015>, 2011.
- Andela, N., Morton, D. C., Giglio, L., Chen, Y., van der Werf, G. R., Kasibhatla, P. S., DeFries, R. S., Collatz, G. J., Hantson, S., Kloster, S., Bachelet, D., Forrest, M., Lasslop, G., Li, F., Maignon, S., Melton, J. R., Yue, C., and Randerson, J. T.: A human-driven decline in global burned area, *Science*, 356, 1356–1362, <https://doi.org/10.1126/science.aal4108>, 2017.
- Baker, A. R., Li, M., and Chance, R.: Trace Metal Fractional Solubility in Size-Segregated Aerosols From the Tropical Eastern Atlantic Ocean, *Global Biogeochem. Cy.*, 34, e2019GB006510, <https://doi.org/10.1029/2019GB006510>, 2020.
- Baldo, C., Ito, A., Krom, M. D., Li, W., Jones, T., Drake, N., Ignatyev, K., Davidson, N., and Shi, Z.: Iron from coal combustion particles dissolves much faster than mineral dust under simulated atmospheric acidic conditions, *Atmos. Chem. Phys.*, 22, 6045–6066, <https://doi.org/10.5194/acp-22-6045-2022>, 2022.
- Bali, K., Mishra, A. K., Singh, S., Chandra, S., and Lehahn, Y.: Impact of dust storm on phytoplankton bloom over the Arabian Sea: a case study during March 2012, *Environmental Science and Pollution Research International*, 26, 11940–11950, <https://doi.org/10.1007/s11356-019-04602-7>, 2019.
- Bazzani, E., Lauritano, C., and Saggiomo, M.: Southern Ocean Iron Limitation of Primary Production between Past Knowledge and Future Projections, *Journal of Marine Science and Engineering*, 11, 272, <https://doi.org/10.3390/jmse11020272>, 2023.
- Bergas-Massó, E., Gonçalves Ageitos, M., Myriokefalitakis, S., Miller, R. L., van Noije, T., Le Sager, P., Montané Pinto, G., and Pérez García-Pando, C.: Pre-Industrial, Present and Future Atmospheric Soluble Iron Deposition and the Role of Aerosol Acidity and Oxalate Under CMIP6 Emissions, *Earths Future*, 11, e2022EF003353, <https://doi.org/10.1029/2022EF003353>, 2023.
- Bergas-Masso, E., Hamilton, D. S., Myriokefalitakis, S., Rathod, S., Gonçalves Ageitos, M., and Pérez García-Pando, C.: Future climate-driven fires may boost ocean productivity in the iron-limited North Atlantic, *Nat. Clim. Change*, 15, 784–792, <https://doi.org/10.1038/s41558-025-02356-4>, 2025.
- Bhargava, S. K., Garg, A., and Subasinghe, N. D.: In situ high-temperature phase transformation studies on pyrite, *Fuel*, 88, 988–993, <https://doi.org/10.1016/j.fuel.2008.12.005>, 2009.
- Blissett, R. S. and Rowson, N. A.: A review of the multi-component utilisation of coal fly ash, *Fuel*, 97, 1–23, <https://doi.org/10.1016/j.fuel.2012.03.024>, 2012.
- Bond, T. C., Streets, D. G., Yarber, K. F., Nelson, S. M., Woo, J.-H., and Klimont, Z.: A technology-based global inventory of black and organic carbon emissions from combustion, *J. Geophys. Res.-Atmos.*, 109, <https://doi.org/10.1029/2003JD003697>, 2004.
- Bond, T. C., Bhardwaj, E., Dong, R., Jogani, R., Jung, S., Roden, C., Streets, D. G., and Trautmann, N. M.: Historical emissions of black and organic carbon aerosol from energy-related combustion, 1850–2000, *Global Biogeochem. Cy.*, 21, <https://doi.org/10.1029/2006GB002840>, 2007.
- Chen, H., Laskin, A., Baltrusaitis, J., Gorski, C. A., Scherer, M. M., and Grassian, V. H.: Coal Fly Ash as a Source of Iron in Atmospheric Dust, *Environ. Sci. Technol.*, 46, 2112–2120, 2012.
- Chen, Y., Wang, Z., Fang, Z., Huang, C., Xu, H., Zhang, H., Zhang, T., Wang, F., Luo, L., Shi, G., Wang, X., and Tang, M.: Dominant Contribution of Non-dust Primary Emissions and Secondary Processes to Dissolved Aerosol Iron, *Environ. Sci. Technol.*, 58, 17355–17363, <https://doi.org/10.1021/acs.est.4c05816>, 2024.
- Chuang, P. Y., Duvall, R. M., Shafer, M. M., and Schauer, J. J.: The origin of water soluble particulate iron in the Asian atmospheric outflow, *Geophys. Res. Lett.*, 32, 4, <https://doi.org/10.1029/2004gl021946>, 2005.
- Danabasoglu, G., Lamarque, J. F., Bacmeister, J., Bailey, D. A., DuVivier, A. K., Edwards, J., Emmons, L. K., Fasullo, J., Garcia, R., Gettelman, A., Hannay, C., Holland, M. M., Large, W. G., Lauritzen, P. H., Lawrence, D. M., Lenaerts, J. T. M., Lindsay, K., Lipscomb, W. H., Mills, M. J., Neale, R., Oleson, K. W., Otto-Bliesner, B., Phillips, A. S., Sacks, W., Tilmes, S., van Kampenhout, L., Vertenstein, M., Bertini, A., Dennis, J., Deser, C., Fischer, C., Fox-Kemper, B., Kay, J. E., Kinnison, D., Kushner, P. J., Larson, V. E., Long, M. C., Mickelson, S., Moore, J. K., Nienhouse, E., Polvani, L., Rasch, P. J., and Strand, W. G.: The Community Earth System Model Ver-

- sion 2 (CESM2), *J. Adv. Model. Earth Sy.*, 12, e2019MS001916, <https://doi.org/10.1029/2019MS001916>, 2020.
- Deng, J., Ma, X., Zhang, Y., Li, Y., and Zhu, W.: Effects of pyrite on the spontaneous combustion of coal, *International Journal of Coal Science & Technology*, 2, 306–311, <https://doi.org/10.1007/s40789-015-0085-y>, 2015.
- Desboeufs, K., Formenti, P., Torres-Sánchez, R., Schepanski, K., Chaboureau, J.-P., Andersen, H., Cermak, J., Feuerstein, S., Laurent, B., Klopper, D., Namwoonde, A., Cazaunau, M., Chevillier, S., Feron, A., Mirande-Bret, C., Triquet, S., and Piketh, S. J.: Fractional solubility of iron in mineral dust aerosols over coastal Namibia: a link to marine biogenic emissions?, *Atmos. Chem. Phys.*, 24, 1525–1541, <https://doi.org/10.5194/acp-24-1525-2024>, 2024.
- Desboeufs, K. V., Sofikitis, A., Losno, R., Colin, J. L., and Ausset, P.: Dissolution and solubility of trace metals from natural and anthropogenic aerosol particulate matter, *Chemosphere*, 58, 195–203, <https://doi.org/10.1016/j.chemosphere.2004.02.025>, 2005.
- Dutta, B. K., Khanra, S., and Mallick, D.: Leaching of elements from coal fly ash: Assessment of its potential for use in filling abandoned coal mines, *Fuel*, 88, 1314–1323, 2009.
- Elliott, H. E., Pependorf, K. J., Blades, E., Royer, H. M., Pollier, C. G. L., Oehlert, A. M., Kukkadapu, R., Ault, A., and Gaston, C. J.: Godzilla mineral dust and La Soufrière volcanic ash fallout immediately stimulate marine microbial phosphate uptake, *Front. Mar. Sci.*, 10, 2023, <https://doi.org/10.3389/fmars.2023.1308689>, 2024.
- Fu, H., Lin, J., Shang, G., Dong, W., Grassian, V. H., Carmichael, G. R., Li, Y., and Chen, J.: Solubility of Iron from Combustion Source Particles in Acidic Media Linked to Iron Speciation, *Environ. Sci. Technol.*, 46, 11119–11127, 2012.
- García-López, N., Ingabire, A. S., Bailis, R., Eriksson, A. C., Isaxon, C., and Boman, C.: Biomass cookstove emissions – a systematic review on aerosol and particle properties of relevance for health, climate, and the environment, *Environ. Res. Lett.*, 20, 053002, <https://doi.org/10.1088/1748-9326/adc615>, 2025.
- Goncalves, C., Alves, C., Evtuygina, M., Mirante, F., Pio, C., Caseiro, A., Schmidl, C., Bauer, H., and Carvalho, F.: Characterisation of PM10 emissions from woodstove combustion of common woods grown in Portugal, *Atmos. Environ.*, 44, 4474–4480, <https://doi.org/10.1016/j.atmosenv.2010.07.026>, 2010.
- Goodarzi, F.: Characteristics and composition of fly ash from Canadian coal-fired power plants, *Fuel*, 85, 1418–1427, <https://doi.org/10.1016/j.fuel.2005.11.022>, 2006.
- Guieu, C., Al Azhar, M., Aumont, O., Mahowald, N., Levy, M., Ethé, C., and Lachkar, Z.: Major Impact of Dust Deposition on the Productivity of the Arabian Sea, *Geophys. Res. Lett.*, 46, 6736–6744, <https://doi.org/10.1029/2019GL082770>, 2019.
- Hamilton, D., Kasoar, M., Bergas-Massó, E., Dalmonech, D., Hantson, S., Lasslop, G., Voulgarakis, A., and Wells, C.: Global Warming Increases Fire Emissions but Resulting Aerosol Forcing is Uncertain, *Nat. Geosci.* [preprint], <https://doi.org/10.21203/rs.3.rs-4567012/v1>, 2024.
- Hamilton, D. S. and Plaas, H. E.: Residential burning is a potentially significant source of soluble iron to the ocean, *Zenodo* [data set], <https://doi.org/10.5281/zenodo.17903186>, 2025.
- Hamilton, D. S., Hantson, S., Scott, C. E., Kaplan, J. O., Pringle, K. J., Nieradzik, L. P., Rap, A., Folberth, G. A., Spracklen, D. V., and Carslaw, K. S.: Reassessment of pre-industrial fire emissions strongly affects anthropogenic aerosol forcing, *Nat. Commun.*, 9, 3182, <https://doi.org/10.1038/s41467-018-05592-9>, 2018.
- Hamilton, D. S., Scanza, R. A., Feng, Y., Guinness, J., Kok, J. F., Li, L., Liu, X., Rathod, S. D., Wan, J. S., Wu, M., and Mahowald, N. M.: Improved methodologies for Earth system modelling of atmospheric soluble iron and observation comparisons using the Mechanism of Intermediate complexity for Modelling Iron (MIMI v1.0), *Geosci. Model Dev.*, 12, 3835–3862, <https://doi.org/10.5194/gmd-12-3835-2019>, 2019.
- Hamilton, D. S., Scanza, R. A., Rathod, S. D., Bond, T. C., Kok, J. F., Li, L., Matsui, H., and Mahowald, N. M.: Recent (1980 to 2015) Trends and Variability in Daily-to-Interannual Soluble Iron Deposition from Dust, Fire, and Anthropogenic Sources, *Geophys. Res. Lett.*, 47, e2020GL089688, <https://doi.org/10.1029/2020GL089688>, 2020a.
- Hamilton, D. S., Moore, J. K., Arneeth, A., Bond, T. C., Carslaw, K. S., Hantson, S., Ito, A., Kaplan, J. O., Lindsay, K., Nieradzik, L., Rathod, S. D., Scanza, R. A., and Mahowald, N. M.: Impact of Changes to the Atmospheric Soluble Iron Deposition Flux on Ocean Biogeochemical Cycles in the Anthropocene, *Global Biogeochem. Cy.*, 34, e2019GB006448, <https://doi.org/10.1029/2019GB006448>, 2020b.
- Hamilton, D. S., Perron, M. M. G., Bond, T. C., Bowie, A. R., Buchholz, R. R., Guieu, C., Ito, A., Maenhaut, W., Myriokefalitakis, S., Olgun, N., Rathod, S. D., Schepanski, K., Tagliabue, A., Wagner, R., and Mahowald, N. M.: Earth, Wind, Fire, and Pollution: Aerosol Nutrient Sources and Impacts on Ocean Biogeochemistry, *Annu. Rev. Mar. Sci.*, 14, 303–330, <https://doi.org/10.1146/annurev-marine-031921-013612>, 2022.
- Hamilton, D. S., Baker, A. R., Iwamoto, Y., Gassó, S., Bergas-Masso, E., Deutch, S., Dinasquet, J., Kondo, Y., Llort, J., Myriokefalitakis, S., Perron, M. M. G., Wegmann, A., and Yoon, J.-E.: An aerosol odyssey: Navigating nutrient flux changes to marine ecosystems, *Elem. Sci. Anth.*, 11, 00037, <https://doi.org/10.1525/elementa.2023.00037>, 2023.
- Hawco, N. J., Conway, T. M., Coesel, S. N., Barone, B., Seelen, E. A., Yang, S.-C., Bundy, R. M., Pinedo-Gonzalez, P., Bian, X., Sieber, M., Lanning, N. T., Fitzsimmons, J. N., Foreman, R. K., König, D., Groussman, M. J., Allen, J. G., Juranek, L. W., White, A. E., Karl, D. M., Armbrust, E. V., and John, S. G.: Anthropogenic iron alters the spring phytoplankton bloom in the North Pacific transition zone, *P. Natl. Acad. Sci. USA*, 122, e2418201122, <https://doi.org/10.1073/pnas.2418201122>, 2025.
- Hedberg, E., Kristensson, A., Ohlsson, M., Johansson, C., Johansson, P.-Å., Swietlicki, E., Vesely, V., Wideqvist, U., and Westerholm, R.: Chemical and physical characterization of emissions from birch wood combustion in a wood stove, *Atmos. Environ.*, 36, 4823–4837, [https://doi.org/10.1016/S1352-2310\(02\)00417-X](https://doi.org/10.1016/S1352-2310(02)00417-X), 2002.
- Hildemann, L. M., Markowski, G. R., and Cass, G. R.: Chemical composition of emissions from urban sources of fine organic aerosol, *Environ. Sci. Technol.*, 25, 744–759, <https://doi.org/10.1021/es00016a021>, 1991.
- Hoesly, R. M., Smith, S. J., Feng, L., Klimont, Z., Janssens-Maenhout, G., Pitkanen, T., Seibert, J. J., Vu, L., Andres, R. J., Bolt, R. M., Bond, T. C., Dawidowski, L., Kholod, N., Kurokawa, J.-I., Li, M., Liu, L., Lu, Z., Moura, M. C. P., O'Rourke, P. R., and Zhang, Q.: Historical (1750–2014) anthropogenic emissions of reactive gases and aerosols from the Com-

- munity Emissions Data System (CEDs), *Geosci. Model Dev.*, 11, 369–408, <https://doi.org/10.5194/gmd-11-369-2018>, 2018.
- Hu, G., Dam-Johansen, K., Wedel, S., and Hansen, J. P.: Decomposition and oxidation of pyrite, *Prog. Energ. Combust.*, 32, 295–314, <https://doi.org/10.1016/j.peccs.2005.11.004>, 2006.
- Itahashi, S., Hattori, S., Ito, A., Sadanaga, Y., Yoshida, N., and Matsuki, A.: Role of Dust and Iron Solubility in Sulfate Formation during the Long-Range Transport in East Asia Evidenced by ¹⁷O-Excess Signatures, *Environ. Sci. Technol.*, 56, 13634–13643, <https://doi.org/10.1021/acs.est.2c03574>, 2022.
- Ito, A. and Miyakawa, T.: Aerosol Iron from Metal Production as a Secondary Source of Bioaccessible Iron, *Environ. Sci. Technol.*, 57, 4091–4100, <https://doi.org/10.1021/acs.est.2c06472>, 2023.
- Ito, A. and Shi, Z.: Delivery of anthropogenic bioavailable iron from mineral dust and combustion aerosols to the ocean, *Atmos. Chem. Phys.*, 16, 85–99, <https://doi.org/10.5194/acp-16-85-2016>, 2016.
- Ito, A., Lin, G., and Penner, J. E.: Radiative forcing by light-absorbing aerosols of pyrogenetic iron oxides, *Sci. Rep.*, 8, 7347, <https://doi.org/10.1038/s41598-018-25756-3>, 2018.
- Ito, A., Myriokefalitakis, S., Kanakidou, M., Mahowald, N. M., Scanza, R. A., Hamilton, D. S., Baker, A. R., Jickells, T., Sarin, M., Bikkina, S., Gao, Y., Shelley, R. U., Buck, C. S., Landing, W. M., Bowie, A. R., Perron, M. M. G., Guieu, C., Meskhidze, N., Johnson, M. S., Feng, Y., Kok, J. F., Nenes, A., and Duce, R. A.: Pyrogenic iron: The missing link to high iron solubility in aerosols, *Sci. Adv.*, 5, 10, <https://doi.org/10.1126/sciadv.aau7671>, 2019.
- Ito, A., Ye, Y., Baldo, C., and Shi, Z.: Ocean fertilization by pyrogenic aerosol iron, *npj Clim. Atmos. Sci.*, 4, 30, <https://doi.org/10.1038/s41612-021-00185-8>, 2021.
- Jahn, L. G., Jahl, L. G., Bland, G. D., Bowers, B. B., Monroe, L. W., and Sullivan, R. C.: Metallic and Crustal Elements in Biomass-Burning Aerosol and Ash: Prevalence, Significance, and Similarity to Soil Particles, *ACS Earth Space Chem.*, 5, 136–148, <https://doi.org/10.1021/acsearthspacechem.0c00191>, 2021.
- Jankowski, J., Ward, C. R., French, D., and Groves, S.: Mobility of trace elements from selected Australian fly ashes and its potential impact on aquatic ecosystems, *Fuel*, 85, 243–256, 2006.
- Johnson, M. S. and Meskhidze, N.: Atmospheric dissolved iron deposition to the global oceans: effects of oxalate-promoted Fe dissolution, photochemical redox cycling, and dust mineralogy, *Geosci. Model Dev.*, 6, 1137–1155, <https://doi.org/10.5194/gmd-6-1137-2013>, 2013.
- Jones, M. W., Abatzoglou, J. T., Veraverbeke, S., Andela, N., Lasslop, G., Forkel, M., Smith, A. J. P., Burton, C., Betts, R. A., van der Werf, G. R., Sitch, S., Canadell, J. G., Santín, C., Kolden, C., Doerr, S. H., and Le Quééré, C.: Global and Regional Trends and Drivers of Fire Under Climate Change, *Rev. Geophys.*, 60, e2020RG000726, <https://doi.org/10.1029/2020RG000726>, 2022.
- Journet, E., Desboeufs, K. V., Caquineau, S., and Colin, J.-L.: Mineralogy as a critical factor of dust iron solubility, *Geophys. Res. Lett.*, 35, <https://doi.org/10.1029/2007gl031589>, 2008.
- Knorr, W., Jiang, L., and Arneth, A.: Climate, CO₂ and human population impacts on global wildfire emissions, *Biogeosciences*, 13, 267–282, <https://doi.org/10.5194/bg-13-267-2016>, 2016.
- Kok, J. F., Storelvmo, T., Karydis, V. A., Adebisi, A. A., Mahowald, N. M., Evan, A. T., He, C., and Leung, D. M.: Mineral dust aerosol impacts on global climate and climate change, *Nat. Rev. Earth Environ.*, 4, 71–86, <https://doi.org/10.1038/s43017-022-00379-5>, 2023.
- Kurusu, M., Sakata, K., Uematsu, M., Ito, A., and Takahashi, Y.: Contribution of combustion Fe in marine aerosols over the northwestern Pacific estimated by Fe stable isotope ratios, *Atmos. Chem. Phys.*, 21, 16027–16050, <https://doi.org/10.5194/acp-21-16027-2021>, 2021.
- Kutchko, B. G. and Kim, A. G.: Fly ash characterization by SEM-EDS, *Fuel*, 85, 2537–2544, 2006.
- Laforest, G. and Duchesne, J.: Stabilization of electric arc furnace dust by the use of cementitious materials: Ionic competition and long-term leachability, *Cement Concrete Res.*, 36, 1628–1634, <https://doi.org/10.1016/j.cemconres.2006.05.012>, 2006.
- Li, C., Liu, W., Jiao, F., Yang, C., Li, G., Liu, S., and Qin, W.: Separation and recovery of zinc, lead and iron from electric arc furnace dust by low temperature smelting, *Sep. Purif. Technol.*, 312, 123355, <https://doi.org/10.1016/j.seppur.2023.123355>, 2023.
- Li, F., Val Martin, M., Andreae, M. O., Arneth, A., Hantson, S., Kaiser, J. W., Lasslop, G., Yue, C., Bachelet, D., Forrest, M., Kluzek, E., Liu, X., Mangeon, S., Melton, J. R., Ward, D. S., Darmenov, A., Hickler, T., Ichoku, C., Magi, B. I., Sitch, S., van der Werf, G. R., Wiedinmyer, C., and Rabin, S. S.: Historical (1700–2012) global multi-model estimates of the fire emissions from the Fire Modeling Intercomparison Project (FireMIP), *Atmos. Chem. Phys.*, 19, 12545–12567, <https://doi.org/10.5194/acp-19-12545-2019>, 2019.
- Li, L., Mahowald, N. M., Kok, J. F., Liu, X., Wu, M., Leung, D. M., Hamilton, D. S., Emmons, L. K., Huang, Y., Sexton, N., Meng, J., and Wan, J.: Importance of different parameterization changes for the updated dust cycle modeling in the Community Atmosphere Model (version 6.1), *Geosci. Model Dev.*, 15, 8181–8219, <https://doi.org/10.5194/gmd-15-8181-2022>, 2022a.
- Li, R.: Volume mean diameters of fly ash and bottom ash samples, Zenodo [data set], <https://doi.org/10.5281/zenodo.17766592>, 2025.
- Li, R., Zhang, H., Wang, F., He, Y., Huang, C., Luo, L., Dong, S., Jia, X., and Tang, M.: Mass fractions, solubility, speciation and isotopic compositions of iron in coal and municipal waste fly ash, *Sci. Total Environ.*, 838, 155974, <https://doi.org/10.1016/j.scitotenv.2022.155974>, 2022b.
- Li, R., Zhang, H., Wang, F., Ren, Y., Jia, S., Jiang, B., Jia, X., Tang, Y., and Tang, M.: Abundance and fractional solubility of phosphorus and trace metals in combustion ash and desert dust: Implications for bioavailability and reactivity, *Sci. Total Environ.*, 816, 151495, <https://doi.org/10.1016/j.scitotenv.2021.151495>, 2022c.
- Li, S., Zhang, B., Wu, D., Li, Z., Chu, S.-Q., Ding, X., Tang, X., Chen, J., and Li, Q.: Magnetic Particles Unintentionally Emitted from Anthropogenic Sources: Iron and Steel Plants, *Environ. Sci. Technol. Lett.*, 8, 295–300, <https://doi.org/10.1021/acs.estlett.1c00164>, 2021.
- Li, W., Xu, L., Liu, X., Zhang, J., Lin, Y., Yao, X., Gao, H., Zhang, D., Chen, J., Wang, W., Harrison, R. M., Zhang, X., Shao, L., Fu, P., Nenes, A., and Shi, Z.: Air pollution–aerosol interactions produce more bioavailable iron for ocean ecosystems, *Sci. Adv.*, 3, e1601749, <https://doi.org/10.1126/sciadv.1601749>, 2017.
- Li, Y., Wang, W., Han, Y., Liu, W., Wang, R., Zhang, R., Zhao, Z., Sheng, L., and Zhou, Y.: Impact of COVID-19 emission reduction on dust aerosols and marine

- chlorophyll-a concentration, *Sci. Total Environ.*, 918, 170493, <https://doi.org/10.1016/j.scitotenv.2024.170493>, 2024.
- Liu, C., Han, G., Hu, B., Geng, F., Liu, M., Dai, S., and Yang, Y.: Fast Screening of Coal Fly Ash with Potential for Rare Earth Element Recovery by Electron Paramagnetic Resonance Spectroscopy, *Environ. Sci. Technol.*, 55, 16716–16722, <https://doi.org/10.1021/acs.est.1c06658>, 2021.
- Liu, L., Li, W., Lin, Q., Wang, Y., Zhang, J., Zhu, Y., Yuan, Q., Zhou, S., Zhang, D., Baldo, C., and Shi, Z.: Size-dependent aerosol iron solubility in an urban atmosphere, *npj Clim. Atmos. Sci.*, 5, 53, <https://doi.org/10.1038/s41612-022-00277-z>, 2022.
- Liu, M., Matsui, H., Hamilton, D. S., Rathod, S. D., Lamb, K. D., and Mahowald, N. M.: Representation of iron aerosol size distributions of anthropogenic emissions is critical in evaluating atmospheric soluble iron input to the ocean, *Atmos. Chem. Phys.*, 24, 13115–13127, <https://doi.org/10.5194/acp-24-13115-2024>, 2024.
- Loaiza, A., Cifuentes, S., and Colorado, H. A.: Asphalt modified with superfine electric arc furnace steel dust (EAF dust) with high zinc oxide content, *Constr. Build. Mater.*, 145, 538–547, <https://doi.org/10.1016/j.conbuildmat.2017.04.050>, 2017.
- Longo, A. F., Feng, Y., Lai, B., Landing, W. M., Shelley, R. U., Nenes, A., Mihalopoulos, N., Violaki, K., and Ingall, E. D.: Influence of Atmospheric Processes on the Solubility and Composition of Iron in Saharan Dust, *Environ. Sci. Technol.*, 50, 6912–6920, <https://doi.org/10.1021/acs.est.6b02605>, 2016.
- López-García, P., Gelado-Caballero, M. D., Patey, M. D., and Hernández-Brito, J. J.: Atmospheric fluxes of soluble nutrients and Fe: More than three years of wet and dry deposition measurements at Gran Canaria (Canary Islands), *Atmos. Environ.*, 246, 118090, <https://doi.org/10.1016/j.atmosenv.2020.118090>, 2021.
- Luo, C., Mahowald, N., Bond, T., Chuang, P. Y., Artaxo, P., Siefert, R., Chen, Y., and Schauer, J.: Combustion iron distribution and deposition, *Global Biogeochem. Cy.*, 22, <https://doi.org/10.1029/2007GB002964>, 2008.
- Machado, J. G. M. S., Brehm, F. A., Moraes, C. A. M., Santos, C. A. d., Vilela, A. C. F., and Cunha, J. B. M. D.: Chemical, physical, structural and morphological characterization of the electric arc furnace dust, *J. Hazard. Mater.*, 136, 953–960, <https://doi.org/10.1016/j.jhazmat.2006.01.044>, 2006.
- Mahowald, N. M., Engelstaedter, S., Luo, C., Sealy, A., Artaxo, P., Benitez-Nelson, C., Bonnet, S., Chen, Y., Chuang, P. Y., Cohen, D. D., Dulac, F., Herut, B., Johansen, A. M., Kubilay, N., Losno, R., Maenhaut, W., Paytan, A., Prospero, J. M., Shank, L. M., and Siefert, R. L.: Atmospheric Iron Deposition: Global Distribution, Variability, and Human Perturbations, *Annu. Rev. Mar. Sci.*, 1, 245–278, <https://doi.org/10.1146/annurev.marine.010908.163727>, 2009.
- Mahowald, N. M., Kloster, S., Engelstaedter, S., Moore, J. K., Mukhopadhyay, S., McConnell, J. R., Albani, S., Doney, S. C., Bhattacharya, A., Curran, M. A. J., Flanner, M. G., Hoffman, F. M., Lawrence, D. M., Lindsay, K., Mayewski, P. A., Neff, J., Rothenberg, D., Thomas, E., Thornton, P. E., and Zender, C. S.: Observed 20th century desert dust variability: impact on climate and biogeochemistry, *Atmos. Chem. Phys.*, 10, 10875–10893, <https://doi.org/10.5194/acp-10-10875-2010>, 2010.
- Mahowald, N. M., Hamilton, D. S., Mackey, K. R. M., Moore, J. K., Baker, A. R., Scanza, R. A., and Zhang, Y.: Aerosol trace metal leaching and impacts on marine microorganisms, *Nat. Commun.*, 9, 2614, <https://doi.org/10.1038/s41467-018-04970-7>, 2018.
- Marafante, M., Bertinetti, S., Carena, L., Fabbri, D., Malandrino, M., Vione, D., and Berto, S.: Chemical characterization and speciation of the soluble fraction of Arctic PM10, *Anal. Bioanal. Chem.*, 416, 1389–1398, <https://doi.org/10.1007/s00216-024-05131-0>, 2024.
- Matsui, H., Mahowald, N. M., Moteki, N., Hamilton, D. S., Ohata, S., Yoshida, A., Koike, M., Scanza, R. A., and Flanner, M. G.: Anthropogenic combustion iron as a complex climate forcer, *Nat. Commun.*, 9, 1593, <https://doi.org/10.1038/s41467-018-03997-0>, 2018.
- McDaniel, M. F. M., Ingall, E. D., Morton, P. L., Castorina, E., Weber, R. J., Shelley, R. U., Landing, W. M., Longo, A. F., Feng, Y., and Lai, B.: Relationship between Atmospheric Aerosol Mineral Surface Area and Iron Solubility, *ACS Earth Space Chem.*, 3, 2443–2451, <https://doi.org/10.1021/acsearthspacechem.9b00152>, 2019.
- Meij, R.: Trace element behavior in coal-fired power plants, *Fuel Process. Technol.*, 39, 199–217, [https://doi.org/10.1016/0378-3820\(94\)90180-5](https://doi.org/10.1016/0378-3820(94)90180-5), 1994.
- Meskhidze, N., Chameides, W. L., and Nenes, A.: Dust and pollution: A recipe for enhanced ocean fertilization?, *J. Geophys. Res.-Atmos.*, 110, <https://doi.org/10.1029/2004JD005082>, 2005.
- Moore, C. M., Mills, M. M., Arrigo, K. R., Berman-Frank, I., Bopp, L., Boyd, P. W., Galbraith, E. D., Geider, R. J., Guieu, C., Jaccard, S. L., Jickells, T. D., La Roche, J., Lenton, T. M., Mahowald, N. M., Maranon, E., Marinov, I., Moore, J. K., Nakatsuka, T., Oschlies, A., Saito, M. A., Thingstad, T. F., Tsuda, A., and Ulloa, O.: Processes and patterns of oceanic nutrient limitation, *Nat. Geosci.*, 6, 701–710, <https://doi.org/10.1038/ngeo1765>, 2013.
- Moreno, N., Querol, X., Andrés, J. M., Stanton, K., Towler, M., Nugteren, H., Janssen-Jurkovicová, M., and Jones, R.: Physicochemical characteristics of European pulverized coal combustion fly ashes, *Fuel*, 84, 1351–1363, 2005.
- Myriokefalitakis, S., Ito, A., Kanakidou, M., Nenes, A., Krol, M. C., Mahowald, N. M., Scanza, R. A., Hamilton, D. S., Johnson, M. S., Meskhidze, N., Kok, J. F., Guieu, C., Baker, A. R., Jickells, T. D., Sarin, M. M., Bikkina, S., Shelley, R., Bowie, A., Perron, M. M. G., and Duce, R. A.: Reviews and syntheses: the GESAMP atmospheric iron deposition model intercomparison study, *Biogeosciences*, 15, 6659–6684, <https://doi.org/10.5194/bg-15-6659-2018>, 2018.
- Nishioka, J. and Obata, H.: Dissolved iron distribution in the western and central subarctic Pacific: HNLC water formation and biogeochemical processes, *Limnol. Oceanogr.*, 62, 2004–2022, <https://doi.org/10.1002/lno.10548>, 2017.
- Oakes, M., Ingall, E. D., Lai, B., Shafer, M. M., Hays, M. D., Liu, Z. G., Russell, A. G., and Weber, R. J.: Iron Solubility Related to Particle Sulfur Content in Source Emission and Ambient Fine Particles, *Environ. Sci. Technol.*, 46, 6637–6644, 2012.
- Oliveira, C. M., Machado, C. M., Duarte, G. W., and Peterson, M.: Beneficiation of pyrite from coal mining, *J. Clean. Prod.*, 139, 821–827, <https://doi.org/10.1016/j.jclepro.2016.08.124>, 2016.
- Ooki, A., Nishioka, J., Ono, T., and Noriki, S.: Size dependence of iron solubility of Asian mineral dust particles, *J. Geophys. Res.-Atmos.*, 114, <https://doi.org/10.1029/2008JD010804>, 2009.

- Panda, P. P., Aswini, M. A., Bhatt, P., Srimuruganandam, B., Peketi, A., and Kumar, A.: Bioactive Trace Elements' Composition and Their Fractional Solubility in Aerosols from the Arabian Sea during the Southwest Monsoon, *ACS Earth Space Chem.*, 6, 1969–1981, <https://doi.org/10.1021/acsearthspacechem.2c00067>, 2022.
- Patil, R. S., Kumar, R., Menon, R., Shah, M. K., and Sethi, V.: Development of particulate matter speciation profiles for major sources in six cities in India, *Atmos. Res.*, 132–133, 1–11, <https://doi.org/10.1016/j.atmosres.2013.04.012>, 2013.
- Perron, M. M. G., Meyerink, S., Corkill, M., Strzelec, M., Proemse, B. C., Gault-Ringold, M., Sanz Rodriguez, E., Chase, Z., and Bowie, A. R.: Trace elements and nutrients in wildfire plumes to the southeast of Australia, *Atmos. Res.*, 270, 106084, <https://doi.org/10.1016/j.atmosres.2022.106084>, 2022.
- Perron, M. M. G., Fietz, S., Hamilton, D. S., Ito, A., Shelley, R. U., and Tang, M.: Preface to the inter-journal special issue “RUSTED: Reducing Uncertainty in Soluble aerosol Trace Element Deposition”, *Atmos. Meas. Tech.*, 17, 165–166, <https://doi.org/10.5194/amt-17-165-2024>, 2024.
- Ram, L. C., Tripathi, P. S. M., and Mishra, S. P.: Mössbauer spectroscopic studies on the transformations of iron-bearing minerals during combustion of coals: Correlation with fouling and slagging, *Fuel Process. Technol.*, 42, 47–60, [https://doi.org/10.1016/0378-3820\(94\)00111-6](https://doi.org/10.1016/0378-3820(94)00111-6), 1995.
- Rathod, S. D., Hamilton, D. S., Mahowald, N. M., Klimont, Z., Corbett, J. J., and Bond, T. C.: A Mineralogy-Based Anthropogenic Combustion-Iron Emission Inventory, *J. Geophys. Res.-Atmos.*, 125, e2019JD032114, <https://doi.org/10.1029/2019JD032114>, 2020.
- Rathod, S. D., Hamilton, D. S., Nino, L., Kreidenweis, S. M., Bian, Q., Mahowald, N. M., Alastuey, A., Querol, X., Paytan, A., Artaxo, P., Herut, B., Gaston, C., Prospero, J., Chellam, S., Hueglin, C., Varrica, D., Dongarra, G., Cohen, D. D., Smichowski, P., Gomez, D., Lambert, F., Barraza, F., Bergametti, G., Rodríguez, S., Gonzalez-Ramos, Y., Hand, J., Kyllönen, K., Hakola, H., Chuang, P., Hopke, P. K., Harrison, R. M., Martin, R. V., Walsh, B., Weagle, C., Maenhaut, W., Morera-Gómez, Y., Chen, Y.-C., Pierce, J. R., and Bond, T. C.: Constraining Present-Day Anthropogenic Total Iron Emissions Using Model and Observations, *J. Geophys. Res.-Atmos.*, 129, e2023JD040332, <https://doi.org/10.1029/2023JD040332>, 2024.
- Riahi, K., van Vuuren, D. P., Kriegler, E., Edmonds, J., O'Neill, B. C., Fujimori, S., Bauer, N., Calvin, K., Dellink, R., Fricko, O., Lutz, W., Popp, A., Cuaresma, J. C., Kc, S., Leimbach, M., Jiang, L., Kram, T., Rao, S., Emmerling, J., Ebi, K., Hasegawa, T., Havlik, P., Humpenöder, F., Da Silva, L. A., Smith, S., Stehfest, E., Bosetti, V., Eom, J., Gernaat, D., Masui, T., Rogelj, J., Strefler, J., Drouet, L., Krey, V., Luderer, G., Harmsen, M., Takahashi, K., Baumstark, L., Doelman, J. C., Kainuma, M., Klimont, Z., Marangoni, G., Lotze-Campen, H., Obersteiner, M., Tabeau, A., and Tavoni, M.: The Shared Socioeconomic Pathways and their energy, land use, and greenhouse gas emissions implications: An overview, *Global Environ. Chang.*, 42, 153–168, <https://doi.org/10.1016/j.gloenvcha.2016.05.009>, 2017.
- Ridley, D. A., Heald, C. L., Kok, J. F., and Zhao, C.: An observationally constrained estimate of global dust aerosol optical depth, *Atmos. Chem. Phys.*, 16, 15097–15117, <https://doi.org/10.5194/acp-16-15097-2016>, 2016.
- Rodríguez, S., Prospero, J. M., López-Darias, J., García-Alvarez, M.-I., Zuidema, P., Nava, S., Lucarelli, F., Gaston, C. J., Galindo, L., and Sosa, E.: Tracking the changes of iron solubility and air pollutants traces as African dust transits the Atlantic in the Saharan dust outbreaks, *Atmos. Environ.*, 246, 118092, <https://doi.org/10.1016/j.atmosenv.2020.118092>, 2021.
- Sakata, K., Kurisu, M., Takeichi, Y., Sakaguchi, A., Tanimoto, H., Tamenori, Y., Matsuki, A., and Takahashi, Y.: Iron (Fe) speciation in size-fractionated aerosol particles in the Pacific Ocean: The role of organic complexation of Fe with humic-like substances in controlling Fe solubility, *Atmos. Chem. Phys.*, 22, 9461–9482, <https://doi.org/10.5194/acp-22-9461-2022>, 2022.
- Scanza, R. A., Hamilton, D. S., Perez Garcia-Pando, C., Buck, C., Baker, A., and Mahowald, N. M.: Atmospheric processing of iron in mineral and combustion aerosols: development of an intermediate-complexity mechanism suitable for Earth system models, *Atmos. Chem. Phys.*, 18, 14175–14196, <https://doi.org/10.5194/acp-18-14175-2018>, 2018.
- Schmidl, C., Marr, I. L., Caseiro, A., Kotianová, P., Berner, A., Bauer, H., Kasper-Giebl, A., and Puxbaum, H.: Chemical characterisation of fine particle emissions from wood stove combustion of common woods growing in mid-European Alpine regions, *Atmos. Environ.*, 42, 126–141, <https://doi.org/10.1016/j.atmosenv.2007.09.028>, 2008.
- Schroth, A. W., Crusius, J., Sholkovitz, E. R., and Bostick, B. C.: Iron solubility driven by speciation in dust sources to the ocean, *Nat. Geosci.*, 2, 337–340, <https://doi.org/10.1038/ngeo501>, 2009.
- Seo, H. and Kim, G.: Anthropogenic Iron Invasion into the Ocean: Results from the East Sea (Japan Sea), *Environ. Sci. Technol.*, 57, 10745–10753, <https://doi.org/10.1021/acs.est.3c01084>, 2023.
- Shi, Z. B., Woodhouse, M. T., Carslaw, K. S., Krom, M. D., Mann, G. W., Baker, A. R., Savov, I., Fones, G. R., Brooks, B., Drake, N., Jickells, T. D., and Benning, L. G.: Minor effect of physical size sorting on iron solubility of transported mineral dust, *Atmos. Chem. Phys.*, 11, 8459–8469, <https://doi.org/10.5194/acp-11-8459-2011>, 2011.
- Silva, V. S., Silva, J. S., Costa, B. d. S., Labes, C., and Oliveira, R. M. P. B.: Preparation of glaze using electric-arc furnace dust as raw material, *Journal of Materials Research and Technology*, 8, 5504–5514, <https://doi.org/10.1016/j.jmrt.2019.09.018>, 2019.
- Souza, C. A. C. D., Machado, A. T., Lima, L. R. P. D. A., and Cardoso, R. J. C.: Stabilization of electric-arc furnace dust in concrete, *Mater. Res.*, 13, 513–519, 2010.
- Srinivas, B., Sarin, M. M., and Kumar, A.: Impact of anthropogenic sources on aerosol iron solubility over the Bay of Bengal and the Arabian Sea, *Biogeochemistry*, 110, 257–268, 2012.
- Stathopoulos, V. N., Papandreou, A., Kanellopoulou, D., and Stournaras, C. J.: Structural ceramics containing electric arc furnace dust, *J. Hazard. Mater.*, 262, 91–99, <https://doi.org/10.1016/j.jhazmat.2013.08.028>, 2013.
- Stoner, O., Lewis, J., Martínez, I. L., Gumy, S., Economou, T., and Adair-Rohani, H.: Household cooking fuel estimates at global and country level for 1990 to 2030, *Nat. Commun.*, 12, 5793, <https://doi.org/10.1038/s41467-021-26036-x>, 2021.
- Tagliabue, A., Aumont, O., and Bopp, L.: The impact of different external sources of iron on the global carbon cycle, *Geophys. Res. Lett.*, 41, 920–926, <https://doi.org/10.1002/2013GL059059>, 2014.

- Tagliabue, A., Bowie, A. R., Boyd, P. W., Buck, K. N., Johnson, K. S., and Saito, M. A.: The integral role of iron in ocean biogeochemistry, *Nature*, 543, 51–59, <https://doi.org/10.1038/nature21058>, 2017.
- Tang, M., Perron, M. M. G., Baker, A. R., Li, R., Bowie, A. R., Buck, C. S., Kumar, A., Shelley, R., Ussher, S. J., Clough, R., Meyerink, S., Panda, P. P., Townsend, A. T., and Wyatt, N.: Measurement of soluble aerosol trace elements: inter-laboratory comparison of eight leaching protocols, *Atmos. Meas. Tech.*, 18, 6125–6141, <https://doi.org/10.5194/amt-18-6125-2025>, 2025.
- Taylor, S. R. and McLennan, S. M.: The geochemical evolution of the continental crust, *Rev. Geophys.*, 33, 241–265, 1995.
- Tegler, L. A., Sherry, A. M., Herckes, P., Romaniello, S. J., and Anbar, A. D.: Up in Smoke: Most Aerosolized Fe from Biomass Burning Does Not Derive From Foliage, *Global Biogeochem. Cy.*, 37, e2023GB007796, <https://doi.org/10.1029/2023GB007796>, 2023.
- Turnock, S. T., Allen, R. J., Andrews, M., Bauer, S. E., Deushi, M., Emmons, L., Good, P., Horowitz, L., John, J. G., Michou, M., Nabat, P., Naik, V., Neubauer, D., O'Connor, F. M., Olivie, D., Oshima, N., Schulz, M., Sellar, A., Shim, S., Takemura, T., Tilmes, S., Tsigaridis, K., Wu, T., and Zhang, J.: Historical and future changes in air pollutants from CMIP6 models, *Atmos. Chem. Phys.*, 20, 14547–14579, <https://doi.org/10.5194/acp-20-14547-2020>, 2020.
- van Marle, M. J. E., Kloster, S., Magi, B. I., Marlon, J. R., Daniau, A.-L., Field, R. D., Arneeth, A., Forrest, M., Hantson, S., Kehrwald, N. M., Knorr, W., Lasslop, G., Li, F., Manguon, S., Yue, C., Kaiser, J. W., and van der Werf, G. R.: Historic global biomass burning emissions for CMIP6 (BB4CMIP) based on merging satellite observations with proxies and fire models (1750–2015), *Geosci. Model Dev.*, 10, 3329–3357, <https://doi.org/10.5194/gmd-10-3329-2017>, 2017.
- Vieira, C. M. F., Sanchez, R., Monteiro, S. N., Lalla, N., and Quaranta, N.: Recycling of electric arc furnace dust into red ceramic, *Journal of Materials Research and Technology*, 2, 88–92, <https://doi.org/10.1016/j.jmrt.2012.09.001>, 2013.
- Wang, R., Balkanski, Y., Boucher, O., Bopp, L., Chappell, A., Ciais, P., Hauglustaine, D., Peñuelas, J., and Tao, S.: Sources, transport and deposition of iron in the global atmosphere, *Atmos. Chem. Phys.*, 15, 6247–6270, <https://doi.org/10.5194/acp-15-6247-2015>, 2015.
- Ward, C. R.: Analysis, origin and significance of mineral matter in coal: An updated review, *Int. J. Coal Geol.*, 165, 1–27, <https://doi.org/10.1016/j.coal.2016.07.014>, 2016.
- Watson, J. G., Chow, J. C., and Houck, J. E.: PM_{2.5} chemical source profiles for vehicle exhaust, vegetative burning, geological material, and coal burning in Northwestern Colorado during 1995, *Chemosphere*, 43, 1141–1151, [https://doi.org/10.1016/S0045-6535\(00\)00171-5](https://doi.org/10.1016/S0045-6535(00)00171-5), 2001.
- Winton, V. H. L., Bowie, A. R., Curran, M. A., and Moy, A. D.: Enhanced Deposition of Atmospheric Soluble Iron by Intrusions of Marine Air Masses to East Antarctica, *J. Geophys. Res.-Atmos.*, 127, e2022JD036586, <https://doi.org/10.1029/2022JD036586>, 2022.
- Wu, C., Lin, Z., and Liu, X.: The global dust cycle and uncertainty in CMIP5 (Coupled Model Intercomparison Project phase 5) models, *Atmos. Chem. Phys.*, 20, 10401–10425, <https://doi.org/10.5194/acp-20-10401-2020>, 2020.
- Wu, D., Li, Q., Ding, X., Sun, J., Li, D., Fu, H., Teich, M., Ye, X., and Chen, J.: Primary Particulate Matter Emitted from Heavy Fuel and Diesel Oil Combustion in a Typical Container Ship: Characteristics and Toxicity, *Environ. Sci. Technol.*, 52, 12943–12951, <https://doi.org/10.1021/acs.est.8b04471>, 2018.
- Wu, H.-Y., Hsieh, C.-C., and Ho, T.-Y.: Trace metal dissolution kinetics of East Asian size-fractionated aerosols in seawater: The effect of a model siderophore, *Mar. Chem.*, 254, 104277, <https://doi.org/10.1016/j.marchem.2023.104277>, 2023.
- Xia, D. K. and Picklesi, C. A.: Microwave caustic leaching of electric arc furnace dust, *Miner. Eng.*, 13, 79–94, [https://doi.org/10.1016/S0892-6875\(99\)00151-X](https://doi.org/10.1016/S0892-6875(99)00151-X), 2000.
- Ye, L., Peng, Z., Ye, Q., Wang, L., Augustine, R., Perez, M., Liu, Y., Liu, M., Tang, H., Rao, M., Li, G., and Jiang, T.: Toward environmentally friendly direct reduced iron production: A novel route of comprehensive utilization of blast furnace dust and electric arc furnace dust, *Waste Management*, 135, 389–396, <https://doi.org/10.1016/j.wasman.2021.08.045>, 2021.
- Zhang, H., Wang, S., Hao, J., Wan, L., Jiang, J., Zhang, M., Mestl, H. E. S., Alnes, L. W. H., Aunan, K., and Melouki, A. W.: Chemical and size characterization of particles emitted from the burning of coal and wood in rural households in Guizhou, China, *Atmos. Environ.*, 51, 94–99, <https://doi.org/10.1016/j.atmosenv.2012.01.042>, 2012.
- Zhang, H., Li, R., Dong, S., Wang, F., Zhu, Y., Meng, H., Huang, C., Ren, Y., Wang, X., Hu, X., Li, T., Peng, C., Zhang, G., Xue, L., Wang, X., and Tang, M.: Abundance and Fractional Solubility of Aerosol Iron During Winter at a Coastal City in Northern China: Similarities and Contrasts Between Fine and Coarse Particles, *J. Geophys. Res.-Atmos.*, 127, e2021JD036070, <https://doi.org/10.1029/2021JD036070>, 2022.
- Zhang, T., Liu, J., Xiang, Y., Liu, X., Zhang, J., Zhang, L., Ying, Q., Wang, Y., Wang, Y., Chen, S., Chai, F., and Zheng, M.: Quantifying anthropogenic emission of iron in marine aerosol in the Northwest Pacific with shipborne online measurements, *Sci. Total Environ.*, 912, 169158, <https://doi.org/10.1016/j.scitotenv.2023.169158>, 2024.